R-01-37

Effects of glacial/post-glacial weathering compared with hydrothermal alteration – implications for matrix diffusion

Results from drillcore studies in porphyritic quartz monzodiorite from Äspö SE Sweden

Ove Landström, Studsvik Ecosafe

Eva-Lena Tullborg, Terralogica AB

Gunda Eriksson, Yvonne Sandell, Studsvik Nuclear

August 2001

Svensk Kärnbränslehantering AB
Swedish Nuclear Fuel
and Waste Management Co
Box 5864
SE-102 40 Stockholm Sweden
Tel 08-459 84 00
+46 8 459 84 00
Fax 08-661 57 19
+46 8 661 57 19

ISSN 1402-3091
SKB Rapport R-01-37

Effects of glacial/post-glacial weathering compared with hydrothermal alteration – implications for matrix diffusion

Results from drillcore studies in porphyritic quartz monzodiorite from Äspö SE Sweden

Ove Landström, Studsvik Ecosafe

Eva-Lena Tullborg, Terralogica AB

Gunda Eriksson, Yvonne Sandell, Studsvik Nuclear

August 2001

Abstract

The effects of hydrothermal + subsequent low temperature alteration and glacial/post-glacial weathering have been studied in two cores of quartz monzodiorite. One core (YA 1192) was drilled into the hydrothermally altered wall rock of a water-conducting fracture exposed at 170 m depth in the access tunnel to the Äspö Hard Rock Laboratory. The other one (Bas 1) was drilled from an outcrop with a glacially polished surface, 1 km north of the YA 1192 site. Both drill cores were sectioned into mm-thick slices perpendicular to the core axis. The fracture filling of the YA 1192 core, the weathered surface of the BAS 1 core and the different slices were analysed for major and trace elements and isotopes of U and Th.

The altered zone of the YA 1192 core extends to approx. 2.5 cm from the fracture surface. The alteration (mainly plagioclase → albite + sericite + epidote) has resulted in a higher porosity and formation of sorbing secondary minerals (e.g. sericite), favouring matrix diffusion. Increased Br concentrations in the altered zone are indicative of saline water in pores and micro fractures i.e. the presence of a diffusion medium. $^{234}U/^{238}U$ activity ratios > 1 and increased Cs in the altered zone are then interpreted as diffusion of U and Cs from fracture groundwater and subsequent sorption. The U migration is geologically recent (< 1 Ma). The 2.5 cm altered zone (corresponding to the zone of active matrix diffusion) significantly exceeds the visible red staining zone (0.5 cm) caused by hematite/FeOOH micrograins, emphasizing the need of microscopy to identify zones of alteration.

The conspicuous weathering at the BAS 1 site is confined to a narrow rim of the bedrock surface (approx. 0.2–0.5 cm thick). Mass balance calculations for this rim (based on immobility of K) indicate that mechanical erosion has dominated over chemical dissolution processes (is roughly 10 times greater). The chemical weathering has affected mainly plagioclase and chlorite resulting in slight dissolution of these minerals. Quartz and K-feldspar have remained almost unaltered. Besides the thin weathered surface rim, slight alteration of plagioclase and increase in porosity is indicated in the 2–3 cm zone below the surface. Decrease of U and Cs concentrations in this zone is then interpreted as being due to leaching/diffusion processes, confined to the Weichselian glaciation (< 100 ka). The $^{234}U/^{238}U$ is close to unity indicating bulk leaching of U under oxic conditions.

The deposition of U in Ya 1192 and leaching of U from BAS 1 are coeval to quaternary glacial, interstadial and interglacial periods during which the hydrogeological and geochemical conditions changed significantly. A main question in performance assessment is whether oxygenated glacial meltwater can penetrate to repository depth (500 m) and modify the redox conditions. The bedrock surface at BAS 1 has certainly been in contact with glacial meltwater as well as meteoric water, resulting in oxidation/ alteration of pyrite, oxidation/mobilisation of U, and probably also desorption/ mobilisation of Cs. In contrast, no signs of oxygenated glacial meltwater influence were found in the YA 1192 core (170 m depth). In fact, the absence of Fe oxyhydroxide but presence of fresh pyrite in the fracture filling and the altered zone at YA 1192 as well as deposition of U are contradictory to interactions with oxidising glacial meltwater from the late glaciations.

Sammanfattning

Effekten av hydrotermal omvandling i kombination med efterföljande lågtemperatur-processer har studerats och jämförts med glacial/post-glacial vittring. Studien har utförts på två borrkärnor av kvarts monzodiorit från Äspö, SE Sverige. Den ena borrkärnan (YA 1192) borrades från en sprickyta exponerad på 170 meters djup i Äspötunneln. Borrkärnan sträckte sig från sprickytan genom hydrotermal-omvandlat sidoberg och vidare in i friskt icke-omvandlat berg. Den andra borrkärnan (BAS 1) borrades i en glacialt polerad häll exponerad på norra Äspö, 1 km norr om den plats där YA 1192 borrades. Båda borrkärnorna sektionerades upp i mm tjocka skivor vinkelrät mot borrkärnan. Sprickbeläggningen i YA 1192 kärnan, den vittrade ytan i BAS 1 och de uppsågade skivorna i de två profilerna analyserades med avseende på huvud- och spårelement samt U och Th isotoper.

Den omvandlade zonen i YA 1192 borrkärnan har en utsträckning av ca. 2,5 cm från sprickytan. En påtaglig omvandling av plagioklas har resulterat i bildningen av sekundära mineral med hög sorptionsförmåga (t ex sericit) och har sannolikt också bidragit till den förhöjda porositet som uppmätts i den omvandlade zonen. Rödfärgning orsakad av mikrokorn av hematit/FeOOH sträcker sig däremot endast ca 5 mm in från sprickan, vilket understryker risken med att bedöma den omvandlade zonens utsträckning enbart från okulärt observerbara färgvariationer. Br, Cs och $^{234}U/^{238}U$ aktivitets-förhållandet visar alla förhöjda värden i den omvandlade zonen jämfört med det icke-omvandlade berget. Detta har tolkats som en sannolik förekomst av salint vatten (Br) i porer och mikrosprickor (dvs indikation på ett diffusionsmedium) och in-diffusion och påföljande sorption av U och Cs från grundvatten som har passerat i sprickan. U-migrationen är geologiskt recent (< 1 miljon år).

Vittringen av BAS 1 är begränsad till en tunn zon närmast ytan (ca 0.2–0.5 cm tjock). Massbalans beräkningar baserade på immobilitet av K indikerar att den mekaniska erosionen har dominerat över den kemiska lakningen (ca 10 gånger högre). Den kemiska vittringen har påverkat i huvudsak plagioklas och klorit och har resulterat i en partiell upplösning av dessa mineral. Kvarts och kalifältspat har däremot inte omvandlats nämnvärt men visar en påtaglig ökning av mikrosprickor nära ytan. Pyritoxidation har dokumenterats i de översta 2 mm som en zon av FeOOH omslutande kärnor av pyrit; däremot är pyritkorn 15 mm ner från ytan inte omvandlade. Förutom den tunna vittringshuden i bergytan har en kemisk lakning av Cs och U kunnat identifieras i en zon som sträcker sig ca. 2 cm ner i berget. En ökad porositet, främst beroende på en ökning av mikrosprickor märks också i den här zonen. Migrationen av U and Cs har antagligen skett under glacial/postglacial tid.

Den recenta depositionen av U i YA 1192 (< 1miljoner år baserat på $^{234}U/^{238}U$ aktivitets-kvoten) sammanfaller med glaciala, interstadiala och interglaciala perioder under vilka signifikanta förändringar i de hydrogeologiska och geokemiska förhållandena på Äspö har ägt rum. Till exempel kan nedpressning/avlastning av berggrunden orsakad av ett tjockt istäcke ha påverkat olika spricksystem. Vidare frigjordes stora mängder glacialt smältvatten i samband med att isarna smälte undan. Hällytan i Bas 1 har säkert varit i kontakt med ett glacialt smältvatten under Weichsel glaciationen. Oxiderande förhållanden och låga halter av organiskt material i det glaciala smältvattnet och efterföljande

nederbördsvatten har sannolikt orsakat den lakning av U, liksom den desorption av Cs som har ägt rum i den övre delen av BAS 1 borrkärnan. I borrkärnan YA 1192 visas i stället motsatsen; ingen omvandling av pyriten samt deponering av U, vilket tolkas som att oxiderande smältvatten inte har påverkat sprickbeläggningen eller berget runt sprickan.

Contents

1 Introduction

Predictions of potential contamination of the geological environment by radionuclide leakage from, for example, a deep repository for radioactive waste, are based on modelling radionuclide transport in the bedrock/groundwater system. In addition to fracture geometry, hydraulic conditions and groundwater chemistry, the retardation of radionuclides caused by water/rock interaction is taken into account. Retardation is caused mainly by two mechanisms:

1 Reactions with the surface of the solid phases in immediate contact with the groundwater (e.g. sorption, ion exchange and precipitation). These solid phases usually constitute a mineral coating on the fracture wall and/or loose material (rock and mineral fragments, clay minerals etc) which fill up the fracture. Mineral compositions, exchange and sorption capacities, porosity etc. of fracture coatings and fillings, usually differ strongly from those of the unaltered wall rock.

2 Diffusion of radionuclides in microfractures and connected pores of the wall rock adjacent to the fractures. This retardation, termed “matrix diffusion” and proposed by Neretnieks /1980/, is more effective in fractures of low transmissivity and also dependent on the properties of the wall rock. For example, alteration of the wall rock adjacent to the fracture may have increased the porosity and generated secondary minerals with high sorption capacities; sorption on these may further retard the radionuclides.

The present study is carried out on drillcore material from Äspö, an island located in the archipelago of the Baltic Sea, 25 km north of Oskarshamn (Figure 1-1). In this area, typical for the Proterozoic crystalline basement, most water-conducting fractures are very old and have hydrothermal precursors. This means that several processes (past as well as on-going) have affected both the fracture coating minerals and the wall rock and usually resulted in a few cm thick altered zone adjacent to the fracture.

Matrix diffusion retardation of elements migrating in fractures has probably been operating throughout the conductive period of the fractures, resulting in increased concentrations for an element in the altered zone bordering the fracture (“positive anomalies”). These may have been overprinted by “negative anomalies”, generated by loss of elements during, for example, alteration processes. Only the net effects of accumulation and leaching will thus be seen in the concentration profiles, and quantitative evaluation of past matrix diffusion retardation therefore may be difficult. However, the study of concentration profiles, perpendicular to the surface of water-conducting fractures is nevertheless a straightforward way to obtain information on the role of matrix diffusion processes in a given environment. In such studies it is important to distinguish between the effects of hydrothermal and low-temperature processes, since only the latter are expected to operate and influence radionuclide migration during the next 100 000 years, under most repository conditions.

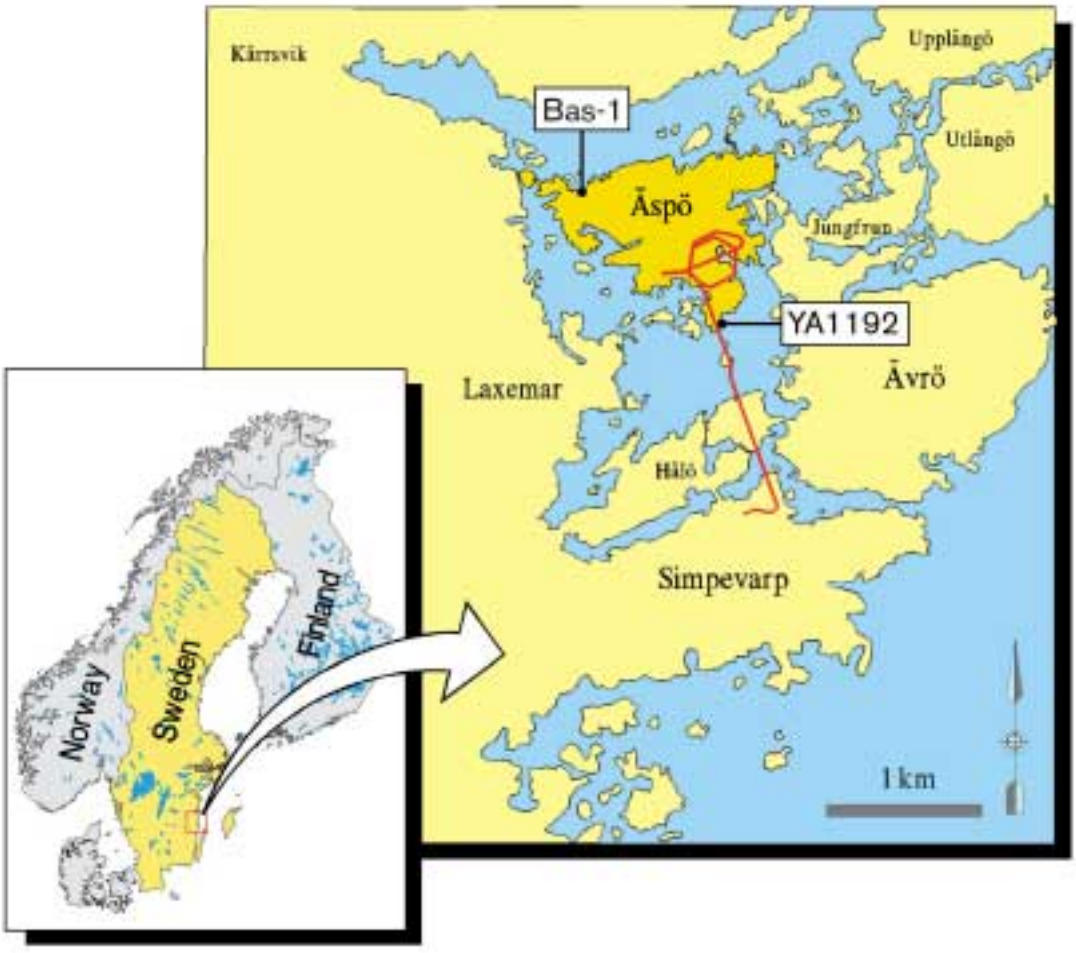

Figure 1-1. *Location of the Äspö site.*

The mobility of some waste radionuclides is highly dependent on the redox conditions; for example, U shows higher mobility under oxidising conditions (as U(VI)) than under reducing conditions (as U(IV)). Reducing conditions at repository depth (approx. 500 m) is thus a presumption for preventing mobilisation of redox-sensitive radionuclides such as U, Tc and Np. The chemistry at this depth is presently reducing but some authors (e.g. King-Clayton et al., 1995 and Glynn et al., 1999) suggest that glacial meltwater enriched in dissolved oxygen may reach repository depths during future glaciations/deglaciations, and possibly change the redox conditions. There are, however, large uncertainties in the parameters used in modelling intrusion of oxygenated meltwater and quite different opinions have been presented /summarised and discussed by Gascoyne, 1999/. Validation of predictions of future intrusion of glacial meltwater and its impact on the redox conditions is thus of great concern. One way is to study responses in fracture minerals and adjacent wall rock to changes in redox conditions associated with the last glaciations.

The main purposes of the present work have been to identify past and present diffusion of elements and natural radionuclides into the wall rock adjacent to a water-conducting fracture, and to study the possible influence of glacial meltwater on redox conditions. In order to disclose low-temperature diffusion components, we have included uranium series disequilibrium studies (confining processes during the recent 1 Ma) and comparative studies of low-temperature glacial/post-glacial weathering.

We have thus studied and compared two extremes of chemical weathering and alteration, both of which have operated in the same rock type:

– hydrothermal + subsequent low temperature alteration of the quartz monzodiorite wall rock adjacent to a water-conducting fracture at 170 m depth in the access tunnel to the Äspö Hard Rock Laboratory.

– low-temperature glacial/post-glacial weathering of an outcropping, glacially polished quartz monzodiorite rock surface on northern Äspö. For locations see Figure 1-1.

2 Geological setting

The dominating rocks in the Äspö area are granitoids, ranging from granite to quartz monzodiorite in composition. They belong to the Trans Scandinavian Igneous Belt (TIB) /Gorbatschev, 1980; cf. also Gaal and Gorbatschev, 1987/, which is regarded as late- to postorogenic in relation to the Svecofennian orogeny. Quartz monzodiorite at Äspö has been dated at 1804 +/- 3 Ma using multigrain zircon and titanite U-Pb dating techniques /Kornfält et al., 1997/.

Xenoliths of basic to intermediate metavolcanics occur in the granitoids and fine-grained alkali granites are present as lenses and dykes. Although generally post-dating the TIB granitoids, most of the fine-grained granites are closely related to these granitoids and have been dated at approximately 1800 Ma /Kornfält et al., 1997/. Some others show distinct contacts and might be associated with the c. 1400 Ma anorogenic Götemar granite which crops out approx. 2 km north of Äspö /Åberg et al., 1984; Smellie and Stuckless, 1985/. Dating results and the determination of a paleomagnetic pole of the Äspö diorite /the latter indicating ages of 1750 Ma; Maddock et al., 1993/ show that it has not been heated above 550–600 °C since the time of crystallisation.

According to Munier /1993/ the earliest fabric in the granitoids of Äspö is a penetrative planar foliation generally trending ENE. Subsequent strain was increasingly localised to block boundaries developing gneissic zones. Later, mylonites segmented the region into blocks. For example, the Äspö island is divided into two blocks by the ENE trending regional shear zone named EW-1. The original foliation is re-oriented and intensified in the mylonites /Munier, 1993/. Brittle deformation later caused fragmentation of the rocks resulting in sets of lineaments trending N-S, E-W, N-E and N-W /Tirén and Beckholmen, 1987; Nisca, 1987/. Most of these faults and fractures are superimposed on older zones of intense foliation or mylonite zones. In contrast to the TIB granitoids and some of the fine-grained granites, the 1400 Ma Götemar granite does not show any regional deformation.

Hydrothermal alteration of the host rock close to the fracture edges is frequently observed /e.g. Eliasson, 1993; Banwart et al., 1994/. Biotite has been altered and replaced by chlorite/epidote, magnetite has been oxidised and hematite/Fe-oxyhydroxide formed. In general, plagioclase is more altered (showing saussuritisation) close to the fracture edges. It is suggested that this alteration is Proterozoic and probably older than 1400 Ma.

The main fracture filling minerals at Äspö are, in order of appearence: chlorite, calcite, epidote, fluorite, quartz, hematite/FeOOH, pyrite and clay minerals. Based on textural relationships the relative ages of the fracture mineralisations have been determined, suggesting the sequence of events presented in Table 2-1 /cf. Landström and Tullborg, 1994; Tullborg et al., 1996/.

Table 2-1. Sequence of tectonic and fracture mineralisation events.

	Formation of the Småland granitoids	c. 1800 Ma (a)
1)	Regional deformation resulting in E-W to ENE-WSW foliation.	
2)	Mylonitisation; formation of fine-grained epidote, muscovite and recrystallisation of quartz.	> 1400 Ma (b)
3)	Reactivation of mylonites and formation of idiomorphic epidote and fluorite.	
4)	Growth of idiomorphic quartz, hematite, fluorite, muscovite, calcite and spherulitic chlorite.	Post magmatic circulation related to the Götemar granite.
5)	Prehnite, laumontite, calcite, chlorite and fluorite.	900–800 Ma (c)
6)	Illite dominated mixed-layer clay, calcite, chlorite? fluorite?	c. 300 Ma (d)
7)	Calcite, Fe-oxyhydroxide, clay minerals?	Recent

(a) Kornfält et al., 1997

(b) Åberg et al., 1984; Smellie and Stuckless, 1985,

(c) Tullborg et al., 1996

(d) Maddock et al., 1993; Tullborg et al., 1995; 1996.

3 Evolution of the bedrock surface at Äspö

According to Lidmar-Bergström /1995/ the Äspö area is part of the Sub-Cambrian peneplain; i.e. the present surface of the bedrock corresponds approximately to the surface exposed during the Vendian/Eocambrian. Since then the surface has been covered by marine and terrestrial sediments of Cambrian to Devonian ages; amounting to 3–4 km in the Äspö area /Tullborg et al., 1995/. During the Permian and early Mesozoic, erosion considerably reduced the thickness of the sediments. However, marine sedimentation most probably took place in the Äspö area during the Cretaceous /Tullborg et al., 1996/. Subsequent uplift reactivated erosion of the sediments but in areas where the Sub-Cambrian peneplain is preserved (e.g. at Äspö) at least a thin cover of sediments remained until the Tertiary.

During the Quaternary several glaciation cycles have influenced the area; the ice has sculptured the bedrock surface and removed earlier weathered surface layers. During the late Weichselian deglaciation (the withdrawing ice passed Äspö approximately 11 900 BP) a till layer was deposited on the Äspö bedrock. Subsequently, the till was covered by alternating fresh and brackish water sediments during the different stages of the Baltic Sea evolution; Baltic Ice Lake (- 10300 BP), Yoldia Sea (- 9500 BP), Ancylus Lake (- 8000 BP) and the Littorina Sea /Björck, 1995/. Due to the progressing crustal uplift following the deglaciation the highest point of Äspö rose above the Sea level about 4000–5000 BP. Till and sediment layers were then successively washed away from the island and only sediments protected in deep depressions were preserved. The present soil cover has thus formed recently and is therefore thin. Especially at high levels of the Äspö island outcropping rocks are still dominant.

The appearance of striations in directions, which coincide with the latest ice progression, implies that the last continental ice has scraped the outcrops. The present surface is thus the result of mechanical erosion and low-temperature chemical weathering during the late (Weichselian) glaciation and the last 4 ka of the post-glacial period. The dominance of outcropping rocks in the higher regions implies a rapid transportation of surface water to the lower parts of the island; either by direct runoff or by infiltration through fractures. This also results in the effective washing away of eroded particles from the rock surface. Due to aggressive humic acids, chemical weathering is more intensive below the locally occurring thin soil cover.

4 Sampling and sample preparation

Two boreholes (parallel and 10 cm apart) were core-drilled perpendicular to a fracture surface exposed on side “A” in the access tunnel to the Äspö Hard Rock Laboratory at chainage 1192 m and at a vertical depth of 170 m (Figure 4-1). The fracture is a water-conducting, single fracture, trending N75°/W65° and the wall has a thin coating of mainly chlorite, clay minerals and calcite. The borehole depth was approximately 1 m and the diameter of the core 5.4 cm. One of the cores, YA 1192, was first sawn along the axis, 0.7 cm from the core centre (Figure 4-2). The smaller segment was saved as reference and also used for preparation of petrographic thin sections. The larger segment was sawn into slices, parallel to the fracture surface. The thin and relatively soft fracture coating on slice A1 was removed using a steel knife and defined as sample A1a. The rest of slice A1 (defined as A1b) and slices A2, A3, A4, A5, A6, A8, A10 and A13, were crushed and homogenised in an agate mortar. The other (parallel) core was used for density and porosity measurements.

Borehole Bas l was core-drilled vertically from the surface of an outcropping rock on northern Äspö to a depth of 0.35 m (Figure 4-1). The core, 5.4 cm in diameter, was sawn and split up into slices similar to that for core YA 1192 (Figure 4-2). From slice B0 the weathered surface (approx. 0.2–0.5 cm thick) was chipped off using a steel chisel, and homogenised in an agate mortar; this sample is defined as $B0_{1+2}$. The rest of slice B0 (defined as $B0_3$) and slices B1, B2, B3, B4, B6 and B8, were crushed and homogenised in an agate mortar.

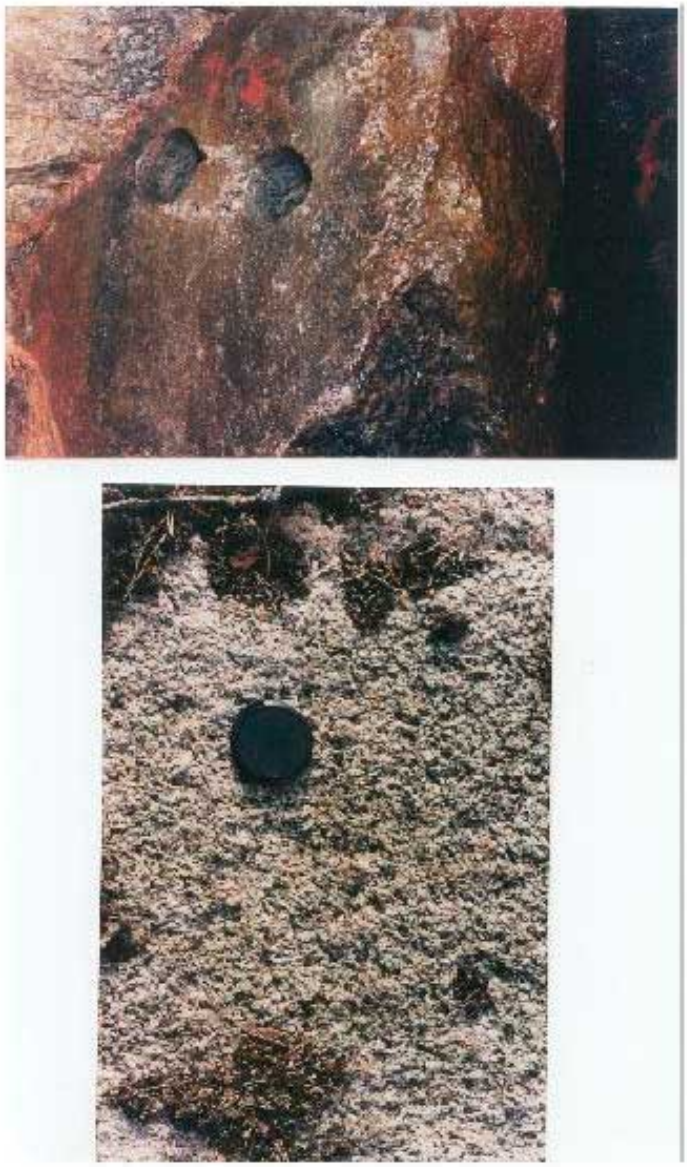

4-1a

4-1b

Figure 4-1.

a. Photo showing fracture surface and the YA 1192 drillholes in the Äspö tunnel.

b. *Photo showing the location for the BAS 1 drillhole on an outcrop 50 m east of borehole KAS 03, northern Äspö.*

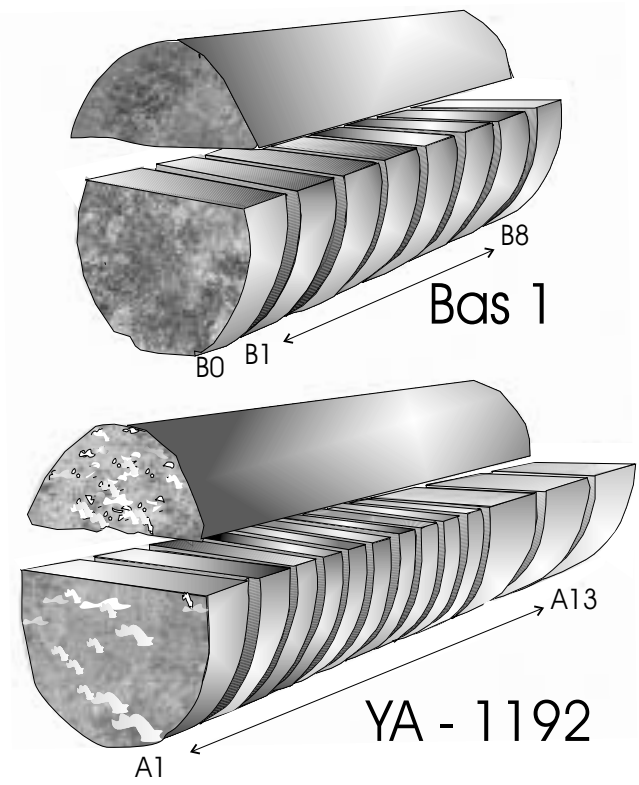

Figure 4-2. *Illustration of the cores BAS 1and YA 1192. The cores were first cut along the axes and the larger segments were then cut into slices parallel to the fracture surfaces. The B0 slice (BAS 1) was divided into* $B0_{1+2}$ *(the weathered surface rim) and* $B0_3$ *(the rest of the upper slice). The A1 slice (YA 1192) was separated into A1a (the fracture coating) and A1b (the slice adjacent to the fracture coating).*

5 Analytical methods

Thin sections were studied using transmissive light polarization microscopy and scanning electron microscopy, the latter for more detailed studies of the weathered surface. Microprobe analyses were carried out on mineral grains of chlorite, biotite and plagioclase. Measurements of connected physical porosity (water saturation) were made at the Swedish National Testing and Research Institute, Borås, Sweden. The samples (drill-core slices in cm thickness) are first dried at 110 °C until a constant weight is reached (minimum 24 h), then stored at room temperature under controlled conditions for 24 hours and finally the dry weight is measured. The sample is then water saturated until stable conditions are achieved, and re-weighed. Following this, the samples are dried a second time and a new dry weight determined.

Subsamples of the powdered sliced material were analysed for major and trace elements using ICP (Inductively Coupled Plasma) and INAA (Instrumental Neutron Activation Analysis), respectively, and for Th and U isotopes by radiochemical separation and alpha-spectrometry. The ICP analyses were carried out at SGAB, Luleå and the INA and Th and U isotope analyses at Studsvik Nuclear, Studsvik, Nyköping.

The combined use of ICP and INAA allows up to 50 elements to be quantitatively determined since precision, accuracy and sensitivity of the two methods generally complement each other. 10–15 elements are determined by both methods allowing some check of analytical quality. Most trace elements of interest in repository performance assessments were included, e.g. Th, U, REEs, Cs and Br. Th and U occur in nuclear waste and are also chemical analogues to Pu and Np, as REEs are to Am and Cm, stable Cs to ^{135}Cs and ^{137}Cs and, in addition, Br can be used as a chemical analogue to I. Moreover, Br turned out to be useful in the present study since it disclosed the existence of saline water in pores and microfractures, i.e. indirectly the extent of the matrix diffusion medium. The INAA technique and the radiochemical methods are described in more detail below.

For INAA, samples of about 200–300 mg were weighed into plastic ampoules and irradiated for 1 hour in a neutron flux of 3×10^{13} n/cm^2 s. Sets of two samples were sequentially irradiated in a selected position. The activity of the radionuclides was determined by gamma ray spectrometry; measurements were carried out after delays of 7 days and 1 month, respectively.

Calibration has been based on pure elements from prepared solutions and on the USGS reference rock standards BCR-1, G-2 and GSP-1. Data on the latter were taken from compilations of certified and recommended concentrations /Govindajaru, 1989/. The standards used for calibration have been irradiated and measured identically to the rock samples. Deviation of the neutron flux from that valid for the standard data set was determined by measurement of a Zr monitor and analysis of a reference (“inhouse”) rock standard, both irradiated identically to the standard and rock samples. These corrections were usually small and mostly < 10%. Each irradiation thus comprised up to 10–15 samples, one Zr monitor and one reference rock standard. The variation of the neutron flux during the irradiation period (approximately 8 hours for all samples) was considered insignificant.

Table 5-1. Results from analyses of the USGS geostandard AGW-1 and comparison with reference values (from Govindajaru, 1989).

Element	n	Average	Std. Dev. %	Reference
Ca %	4	3.2	3.5	3.53
Na	5	3.09	1.7	3.16
K	2	2.7	–	2.42
Fe	5	4.76	2.1	4.73
Rb ppm	5	73.1	7.1	67.3
Cs	5	1.31	3.3	1.28
Sr	5	478	17	662
Ba	5	1170	11	1226
Cr	5	9.1	7.1	10.1
Co	5	15.8	2.6	15.3
Zn	4	90.1	7.5	88
Sb	5	4.2	3.7	4.3
Zr	5	228	10	227
Hf	5	5.1	2.1	5.1
Ta	5	0.90	3.2	0.90
Th	5	6.58	2.1	6.5
U	5	1.88	15	1.92
Sc	5	12.2	2.2	12.2
La	5	37.8	2.7	38
Ce	5	63.9	9.6	67
Nd	5	29.3	9.3	33
Sm	5	5.86	4.1	5.9
Eu	5	1.50	3.8	1.64
Gd	2	5.5	–	5.0
Tb	5	0.84	9.1	0.70
Yb	5	1.86	6.0	1.72
Lu	5	0.28	6.4	0.27

Note that the difference of the average and reference values is taken as a measure of accuracy and the standard deviation as a measure of precision.

n = number of analyses.

Precision and accuracy of the method have been determined by repeated analyses of the USGS rock standard AGW-1 (andesite). Averages of concentrations from the analyses are compared with recommended values in Table 5-1. The difference of the average and recommended values is taken as a measure of accuracy and the standard deviation of the average as a measure of precision. As based on different irradiation occasions the accuracy and precision given in Table 5-1 should be representative of the different sources of errors involved; preparation of the sample for irradiation (weighing etc), correction of neutron flux variation, gamma peak evaluation, counting statistics, variation in sample – standard geometry etc. Both accuracy and precision are, however, to some extent dependent on the matrix and the concentration levels of the sample. For example, the precision of U was 3.0% in the analyses of the U-rich (28 ppm) geostandard ASK 2 compared with 15% in the analysis of the U-poor (1.9 ppm) geostandard AGW-1.

Thorium and uranium isotopes were analysed in selected slices of the YA 1192 and BAS 1 cores using isotope dissolution and alpha spectrometry techniques. Powdered material was digested in teflon beakers with concentrated hydrofluoric, nitric and hydrochloric acids. ^{232}U and ^{229}Th traces were added to the samples before the decomposition processes, for determination of chemical recovery. The thorium and uranium isotopes were separated from the final solutions using conventional extraction and ion exchange techniques, electrodeposited on stainless steel plates and counted by alpha spectrometry. The chemical recovery varied between 12 and 63% for U and between 12 and 90% for Th. The precision varied between 5 and 15% as based on counting statistics.

The same fine-grained material from the YA 1192 core was used in the INA and radiochemical (alpha spectrometry) analyses of U and Th, allowing for comparison of the concentration values (Table 6-3). The agreement between INAA and alpha spectrometry results is good for Th whereas alpha spectrometry shows approx. 10% higher values for U. The large difference in the U concentrations for the fracture coating (15 and 24 ppm for alpha spectrometry and INAA, respectively; Table 6-3) is probably due to low sample weight in the alpha spectrometry analysis (0.06 g) leading to lower accuracy.

6 Results and evaluation of data

The results from the two cores are treated and discussed separately but in order to facilitate comparison, similar YA 1192 and BAS l plots are illustrated in the same figure.

6.1 Core YA 1192

6.1.1 Rock and fracture mineralogy

The rock is a porphyric quartz monzodiorite with the following mineralogical composition of the unaltered rock; plagioclase (42%), quartz (15%), K-feldspar (22%), biotite (15%) and hornblende (3%). Accessory minerals include titanite (1–2%), zircon (< 1%) and apatite (< 1%). Hydrothermal processes have affected the wall rock adjacent to the fracture; evidenced mainly by breakdown of magnetite and alteration of plagioclase. The breakdown of magnetite has resulted in formation of micrograins of hematite (through oxidation of Fe) visualised as a thin (5 mm) red stained rim immediately adjacent to the fracture surface. Plagioclase has been altered to albite + epidote + sericite (+ calcite). This alteration is most intense within the red stained zone but extends 2–3 cm into the wall rock. The Na/Ca atomic ratio of unaltered plagioclase in the YA 1192 core is 2.8 (oligoclase) whereas altered plagioclase has a Na/Ca ratio of about 30 (albite). Photos showing altered and fresh plagioclase are shown in Figure 6-1.

For most hydrothermally altered samples analysed from Äspö there is a connection between the alteration of plagioclase and the breakdown of biotite /e.g. Eliasson, 1993; Landström and Tullborg, 1995/. It is therefore notable that despite the hydrothermal alteration, biotite has been preserved in the wall rock adjacent to fracture YA 1192. Microprobe analyses of biotite close to the fracture edge and at greater distances from the fracture edge show the same chemical composition. These data are also similar to results from, for example, fresh rock samples adjacent to the “Redox zone” (cf. Table 6-1).

The fracture coating is very thin (< 1 mm) and consists of an inhomogeneous layer of dominantly chlorite and minor amounts of calcite, fluorite and some crystals of pyrite. The pyrite has remained fresh and shows no signs of oxidation (Figure 6-2). A few micrometres thick layer of clay covers the surface. It has not been possible to make a straightforward identification of this clay but it is a Fe/Mg clay of smectite- or mixed-layer-clay type. This clay layer constitutes the immediate water/mineral contact.

Porosity measurements, based on water absorption, were carried out in five subsamples from the core parallel to the analysed YA 1192 core. They showed a decrease in porosity with increasing distance from the fracture (from 1.34 to 0.42 volume %, cf. Figure 6-3). The spatial porosity distribution and mineral specific characteristics within the fresh Äspö diorite have been studied by Johansson et al. /1998/ and Byegård et al. /1998/, using the 14-C PMMA impregnation method and autoradiogrammes.

Upper

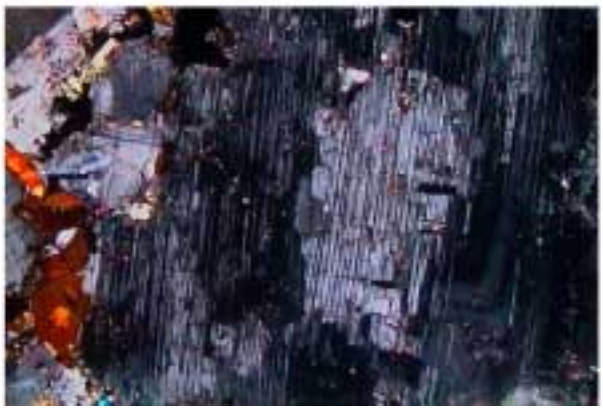

Lower

Figure 6-1. *Photomicrographs from the YA1192 core. Upper: completely altered plagioclase (albite+ acicular epidote and sericite) at a distance of approximately 5 mm from the fracture surface. Lower: relatively fresh twinned plagioclase (oligoclase) at a distance of 25–30 mm from the fracture surface. Length of photos correspond to 2.5 mm.*

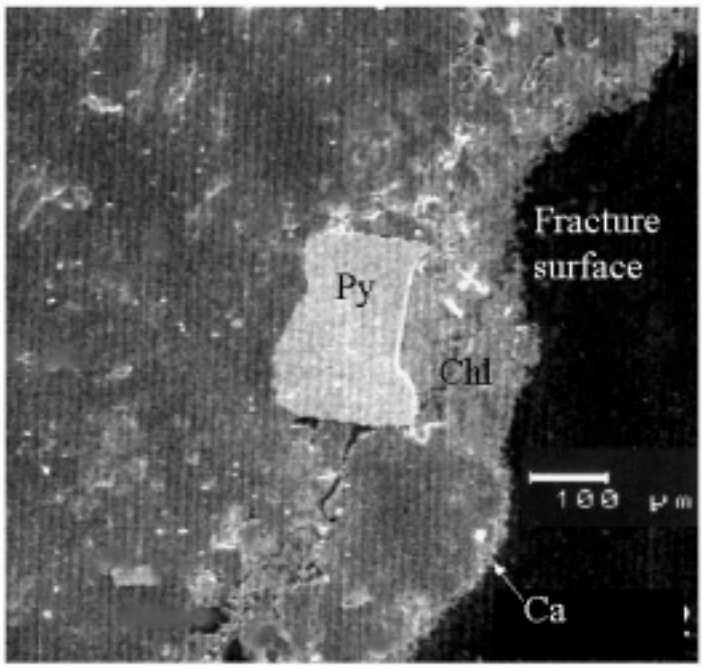

Figure 6-2. *SEM image showing pyrite (Py) and fracture coating of chlorite (Chl) and calcite (Ca) from YA 1192. Note that the pyrite grain shows no sign of alteration.*

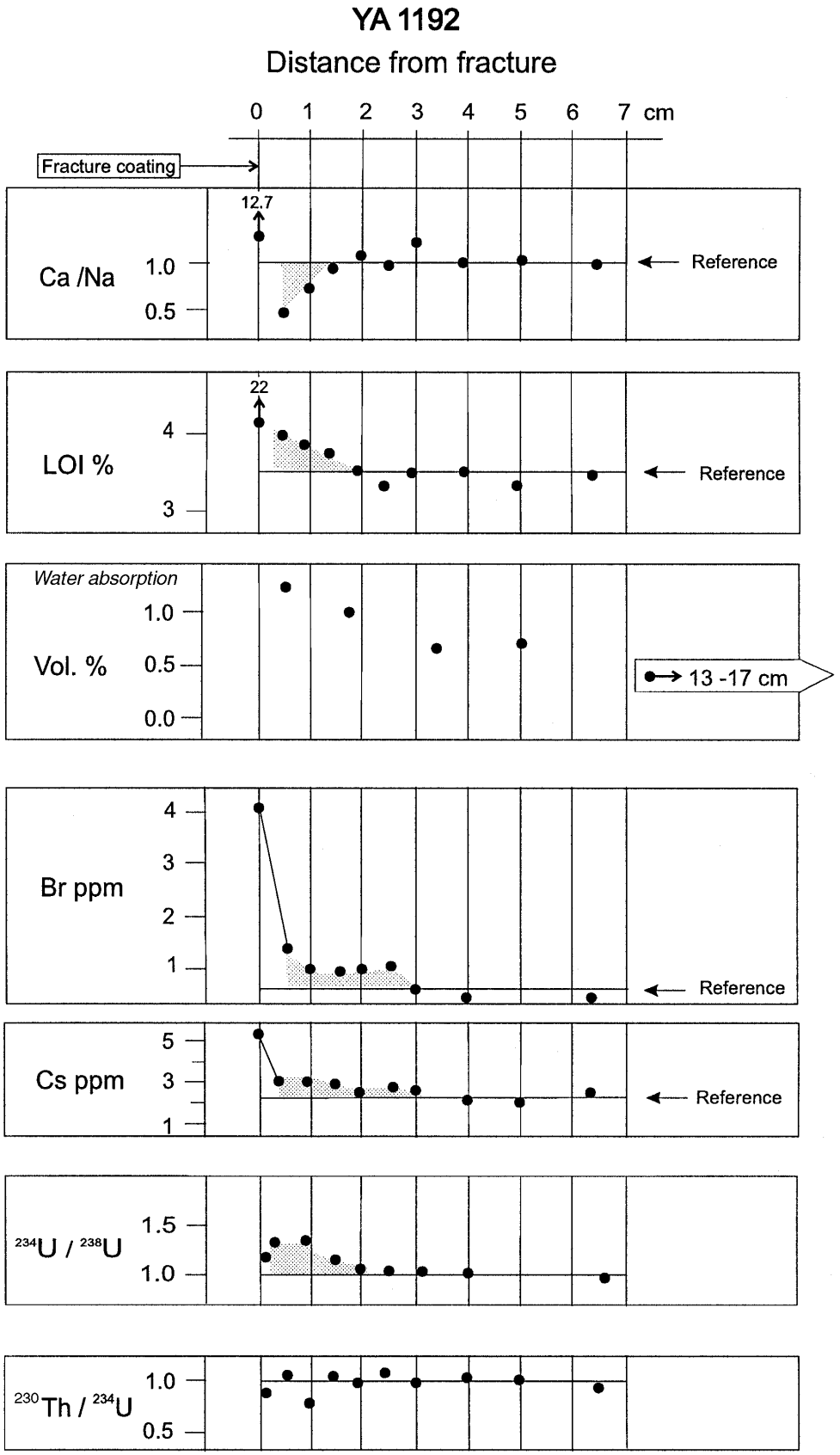

Figure 6-3. *Depth profiles of Ca/Na ratio, LOI, porosity, Br, Cs, $^{234}U/^{238}U$ and $^{230}Th/^{234}U$ activity ratios in core YA 1192. The reference levels are average values of samples A8, A10 and A13 (assumed to be representative of unaltered host rock).*

Table 6-1. EDS analyses of wall rock chlorite, chlorite/clay from the fracture filling in YA 1192 and plagioclase and biotite from fresh samples.

Weight%	MgO	MnO	FeO	Al_2O_3	SiO_2	K_2O	CaO	Na_2O
Chlorite								
Bas 1	18.1	0.5	21.2	16.0	30.2			
The Redox zone*	18.0	0.6	21.5	18.6	28.4			
Chlorite/clay**								
YA 1192	14.6	0.6	16.4	13.0	28.5	2.8	6.5	0.6
YA 1192	19.0	0.6	19.8	16.3	33.1	1.9	0.2	0.9
Plagioclase (fresh)								
BAS				25.5	60.1	0.8	5.3	8.7
YA1192				25.5	61.5	0.2	6.0	8.8
The Redox zone				23.1	62.2	0.1	4.8	9.0
Biotite								
YA1192	0.6	13.1	18.0	14.5	37.0	9.7		0.1
The Redox zone	0.6	12.4	17.5	15.3	38.3	9.4		0.1

* sample from altered wall rock.
** semiquantitative analyses of outermost part of the fracture coating.

Quartz and K-feldspar were identified as non-porous minerals by this method and the connected porosity was identified as a network consisting of microfractures and more porous minerals (plagioclase, biotite and chlorite). The same total porosity was measured in these samples (0.4 ± 0.1 volume %) as in fresh samples from the YA 1192 core. Based on the microscopy of the YA1192 core and the investigation by Siitari-Kauppi (op. cit.) it is expected that the increase in porosity in the altered zone be related to alteration of minerals and formation of microfractures.

6.1.2 Geochemistry

General

Concentrations of major and trace elements and loss on ignition (LOI) values are presented in Table 6-2 and activities and activity ratios of U and Th isotopes in Table 6-3. Average concentrations of samples A8, A10 and A13 (located > 4 cm from the fracture surface) are assumed to be representative of unaltered host rock and referred to as "reference rock".

Table 6-2. Major (in %) and trace element (in ppm) concentrations for samples from the YA 1192 core. Sample A1a represents the fracture coating and sample A1b the slice adjacent to fracture.

Element	A1a	A1b	A2	A3	A4	A5	A6	A8	A10	A13
$Si0_2$ %	29.9	58.8	57.8	57.3	58	59.6	58.2	58.8	60.0	58.0
Al_2O_3	10.2	17.8	17.3	16.7	17.1	17.3	17.8	17.9	17.6	17.9
CaO	12.0	2.84	3.56	4.16	4.64	4.25	3.98	4.66	4.37	4.66
Fe_2O_3	12.6	5.19	5.49	6.82	6.16	4.98	5.2	4.82	5.00	5.60
K_2O	1.93	3.51	3.61	3.10	2.70	3.44	4.20	2.82	3.25	3.25
MgO	8.31	2.00	2.39	2.54	2.40	2.11	2.19	2.22	2.11	2.37
MnO	0.317	0.080	0.089	0.100	0.099	0.086	0.086	0.089	0.085	0.095
Na_2O	0.91	5.51	4.66	4.43	4.35	4.23	4.18	4.63	4.50	4.57
P_2O_5	0.14	0.345	0.375	0.366	0.376	0.329	0.328	0.328	0.310	0.357
TiO_2	1.11	0.753	0.920	0.845	0.952	0.780	0.809	0.848	0.743	0.863
LOI	22.1	4.1	3.9	3.8	3.6	3.2	3.4	3.5	3.2	3.4
Rb ppm	92.7	110	132	113	91	85.5	104	92.2	98.9	93.1
Cs	5.39	3.13	3.3	3.12	2.58	2.63	2.48	2.16	2.01	2.41
Be	3.61	2.51	2.29	2.39		2.48	1.99	2.23		
Sr	169	1120	1320	1260	1250	1320	1320	1320	1300	1320
Ba	408	1822	1870	1452	1325	2273	2819	1545	1874	1917
V	221	93.7	91.2	115	109	84.6	92.0	81.0	85.8	96.3
Cr	196	41.4	44.2	67.3	56.8	42.6	39.3	30.4	42.1	43.1
Co	77.9	14.9	12.2	15.7	16.9	13.3	13.0	12.6	12.7	13.4
Ni	72.4	21.3	25.8	31.4		23.3	23.0	19.5	25.8	25.5
Cu	197	85	85.6	62.7	61	80	92.4	104	92.2	62.9
Zn	385	58.7	63.6	73.6	75.6	59.9	52.3	51.0	47.7	56.9
Br	4.1	1.43	0.87	0.96	0.98	1.07	0.62	0.41		0.54
Zr	35.4	298	224	231	247	249	210	254	224	227
Hf	0.8	6.79	6.74	6.75	7.19	5.79	5.77	5.73	5.07	6.46
Nb										
Ta		0.92	1.12	0.76	1.07	1.0	0.92	0.8	0.75	0.86
Th	1.3	7.0	8.2	7.1	8.1	9.1	6.0	7.5	6.3	8.3
U	24.4	3.1	2.3	2.7	2.6	2.8	2.6	1.7	2.0	3.7
Sc	30.8	9.4	10.2	13.6	12.2	10.3	9.89	11.3	10.3	11.8
La	12.7	52.3	54.4	47.5	55.2	47.3	47.6	54.6	48.9	56.1
Ce	30.9	89.1	137	120	137	114	121	127	107	140
Nd		35.2	61.6	51.0	61.5	54	46.3	55.0	48.4	65.0
Sm	6.70	6.77	9.68	8.42	11.2	8.49	8.92	9.18	8.38	9.43
Eu	1.38	1.50	2.02	1.8	2.15	1.64	1.85	1.94	1.67	1.96
Tb	0.87	0.97	1.16	1.2	1.13	0.97	1.02	1.33	0.96	1.32
Yb	2.28	2.47	2.52	2.4	2.41	1.85	2.00	2.18	1.99	2.25
Lu	0.43	0.24	0.37	0.33	0.34	0.26	0.29	0.27	0.28	0.30
Y	20.8	20.7	20.4	16.9	23.7	18.0	18.6	21.1	16.6	21.0

Values of reference rock (not shown in the table) are averages of samples A8, A10 and A13.

Table 6-3. Concentrations of Th and U (INAA and alpha-spectrometry) and activity ratios for the YA1192 core.

Sample number	Th (ppm)		U (ppm)		$^{234}U/^{238}U$	$^{230}Th/^{234}U$	$^{228}Th/^{232}Th$
	INAA	alpha-sp.	INAA	alpha-sp.			
A1a	1.3	n.d.	24.4	15.1	1.14	0.93	11.1
A1b	7.0	8.4	3.1	3.6	1.33	0.99	1.00
A2	8.2	7.4	2.3	3.1	1.34	0.90	1.17
A3	7.1	7.6	2.7	2.8	1.12	0.99	1.17
A4	8.1	8.9	2.6	3.1	1.05	0.99	1.11
A5	9.1	8.9	2.8	2.8	1.02	1.08	0.97
A6	6.0	6.3	2.6	2.5	1.04	1.02	1.16
A8	7.5	8.1	1.7	2.8	1.08	1.03	1.16
A10	6.3	6.5	2.0	2.7	1.00	1.08	0.99
A13	8.3	8.1	3.7	4.1	0.95	0.97	1.13

The chemical composition of the fracture coating differs strongly from that of the wall rock. Relative to reference rock, the fracture coating (sample A1a in Table 6-2) is enriched in U (by a factor of 10), Br (8.3), Zn (7.4), Co (5.8), Mg and Mn (3.6), Ca, Fe, Sc, V, Ni and Cs (2.3–3.1) and Ti (1.4). The coating is depleted in Si, Al and K (0.51–0.61), light REEs (0.25 for La), Na, Sr, Ba, Zr, Hf and Th (0.13–0.20). Only Rb, heavy REEs and Y are about equal in the fracture coating and reference rock. These differences disclose the dominance of certain minerals in the fracture coating, e.g. calcite (Ca), chlorite (Fe, Mg) and pyrite (Fe), low content of accessory minerals (REEs, Zr, Hf and Th), high porosity (Br dissolved in the pore water) as well as sorption processes (U and Cs).

Geochemical indications of altered zones, matrix diffusion, saline pore water and redox conditions

Deviations from reference rock values in the Ca/Na concentration ratio, LOI, water absorption, Br and Cs concentrations and the $^{234}U/^{238}U$ activity ratio were observed in a 2–3 cm thick zone adjacent to the fracture surface. Depth profiles of these parameters, suggested to indicate altered zones with increased porosity and matrix diffusion of Cs and U, are illustrated in Figure 6-3.

Alteration

– Relative to reference rock the concentration of Ca is low in the wall rock adjacent to the fracture (Table 6-2) and the Ca/Na ratio decreases towards the fracture surface, starting within about 2 cm of the fracture surface (Figure 6-3). This suggests leaching of Ca in connection with alteration of plagioclase to albite and subsequent transfer to secondary mineral phases in the altered zone (e.g. epidote and calcite) and the fracture coating (that shows high Ca and Ca/Na values; Table 6-2 and Figure 6-3), or removal by fracture groundwater. This element loss from the wall rock results in a decrease in density and increase in pore space; i.e. generates conditions favourable to matrix diffusion. Porosity values of 1.34 and 1.08 volume % were thus measured in the altered zone, as compared to 0.4 volume % for unaltered rocks (Figure 6-3, see also section 6.1.1).

– LOI increases towards the fracture surface, starting within 2–2.5 cm of the fracture surface from a background level of about 3.4, and reaching 4.1 in sample A1b and 22.1 in the fracture coating (Table 6-2 and Figure 6-3). The increased LOI values are attributed to "crystal-bound" water and indicate the presence of secondary mineral phases (e.g. sericite and clay minerals) but possibly also a somewhat higher H_2O content in the biotite.

Matrix diffusion

– Br increases from a background level of about 0.5 ppm (reference rock) to about 1 ppm in the altered zone and to 4.1 ppm in the fracture coating (Table 6-2 and Figure 6-3). Br is a conservative, non-reactive element, and is usually present in low concentrations in crystalline rocks /< 0.5 ppm, see Govindajaru, 1989/ where it mainly occurs in fluid inclusions /Nordström et al., 1989/. It is suggested that the fraction of Br exceeding the background level is mainly contained in saline water in connected pores and microfractures and thus indicates increased porosity as well as the presence of a diffusion medium in the 2.5 cm zone adjacent to the fracture surface.

– Cs is highest in the fracture coating (5.4 ppm) and significantly higher in the altered zone than in the reference rock. (Table 6-2 and Figure 6-3). This suggests retardation of Cs transported in fracture groundwater, by diffusion in microfractures and pores of the altered zone, and subsequent sorption onto secondary minerals. This interpretation is supported by the Cs/K ratio profile in Figure 7-1 (c.f. discussion in section 7.2).

– The $^{234}U/^{238}U$ activity ratios exceed unity in the altered zone adjacent to the fracture surface (Table 6-3 and Figure 6-3) indicating geologically recent deposition of U (< ≈ 1 Ma). The $^{234}U/^{238}U$ "anomaly" coincides with those of Ca/Na, LOI and Br and it is suggested that uranium was supplied to the altered zone by diffusion in pores and microfractures. The $^{230}Th/^{234}U$ activity ratios are close to unity suggesting either a very slow diffusion rate of U during the last 0.35 Ma (allowing ingrowth of ^{230}Th), or an episodic event of U deposition occurring > 0.35 Ma ago. Although the excess ^{234}U indicates deposition of uranium in an approximately 2 cm thick zone (Figure 6-3), there is no corresponding increase in the uranium content (or decrease in the Th/U weight ratio). This could be explained by earlier leaching of uranium, possibly in connection with the alteration processes, or, alternatively, that the amount of U deposited was small but had a high $^{234}U/^{238}U$ activity ratio.

Saline pore water

From a measured mean porosity of 1.2 volume % for the altered 0–2.5 cm zone and an excess Br concentration of 0.5 ppm (i.e. the concentration of Br exceeding the reference rock value), a concentration in the order of 100 ppm is estimated for Br in the pore water. This implies a salinity in the range of 15 000–20 000 ppm Cl, as based on a Cl/Br ratio of 150–200, typical of saline groundwater at Äspö. The salinity of the associated fracture groundwater during undisturbed conditions is probably lower. Due to serious disturbance by the tunnel construction, groundwater from the fracture has not been analysed.

The presence of saline water in less transmissive parts (rock matrix) of a crystalline rock aquifer has been demonstrated in Canada /Gascoyne, 1996/ where water of 90 g/l TDS was found. Similar studies are presently carried out within the Matrix Fluid Experiment at Äspö; leaching of drillcore samples and sampling of groundwater from extremely low transmissive sections intersected by a borehole at 450 metres depth /Smellie, 2000/.

Past and present redox conditions

Hydrothermal (old) oxidation has affected the wall rock adjacent to the fracture, leading to breakdown of magnetite and formation of micro-grains of hematite, visible as a thin (5 mm) red stained rim immediately adjacent to the fracture surface. Subsequently pyrite has precipitated on the fracture wall. The presence of fresh pyrite in the fracture coating, 100–200 μm from the fracture edge (Figure 6-2) and the recent ($< \approx 1$ Ma) deposition of uranium in the fracture coating and adjacent wall rock indicate reducing conditions during recent time.

Behaviour of other elements

Ti, Zr and Hf

Ti generally occurs in the resistant minerals ilmenite and rutile, in titanite and in rock-forming minerals (e.g. hornblende and biotite); Zr and Hf are predominantly contained in zircon. Due to their presence in resistant minerals or tendency to remain in secondary mineral phases in connection with alteration (Ti), these elements are frequently applied as immobile conservative elements in calculations of mass changes in weathering processes /e.g. Nesbitt, 1979/. They behave, however, differently in the YA 1192 core. Mobilisation of Ti is thus indicated by increased concentration in the fracture filling and decreased concentration in the slice immediately adjacent to the fracture (1.11 and 0.75% TiO_2, respectively, as compared to 0.82% for reference rock). In contrast, Zr and Hf vary little in the wall rock samples but are significantly lower in the fracture coating (approximately one sixth of the reference rock values). This contrasting behaviour of Ti relative to Zr and Hf is illustrated in Figure 6-4 showing plots of Ti versus Hf.

It is suggested that Zr and Hf in the fracture coating are hosted in zircons released in connection with alteration processes in the outermost zone of the wall rock. In contrast, Ti was probably mobilised in hydrothermal alteration/dissolution of titanite in the outer wall rock and formed secondary minerals in the fracture coating, as illustrated in Figure 6-5.

Th, REEs and Y

Th and La (representing light REEs) show similar trends and distributions as do Zr and Hf; they are approximately constant in the wall rock but decrease to one sixth and one fourth, respectively, in the fracture coating (Table 6-2). In contrast, Yb (representing heavy REEs) and Y show similar concentrations in the fracture coating and in the wall rock (cf. Table 6-2 and chondrite-normalised REE patterns in Figure 6-6). Part of the REEs (especially light REEs) and Th in the fracture coating may be associated with apatite. Since apatite is the only P-containing mineral observed, the concentration of phosphorus in the coating (0.14% P_2O_5 compared to 0.35% in the host rock), reflects the amount of this mineral.

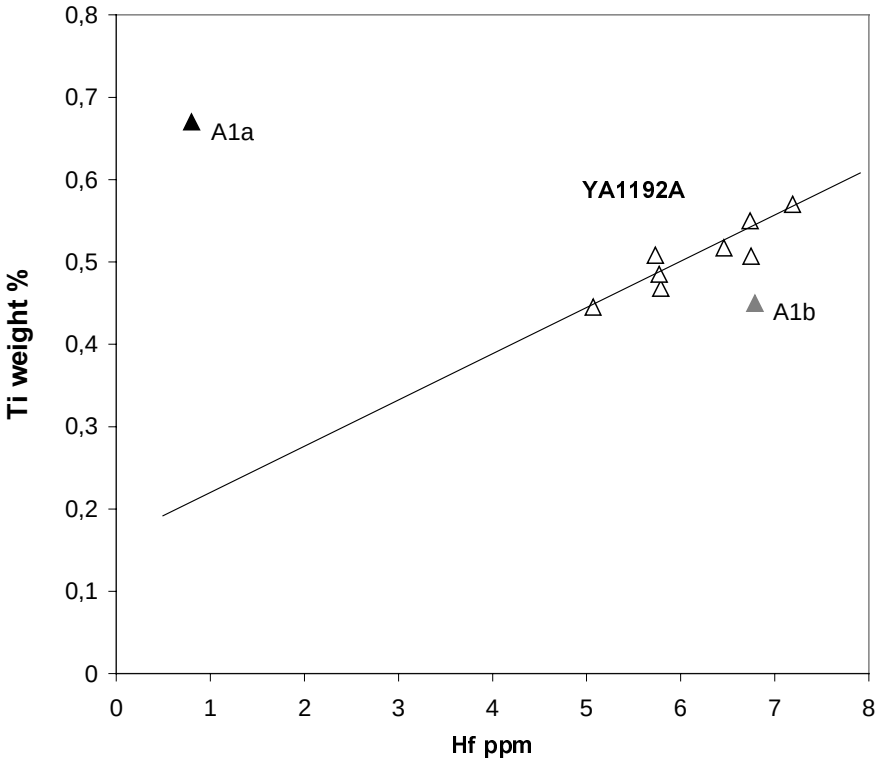

Figure 6-4. *Plot of Ti versus Hf for slices from the YA 1192 core. Note the increase of Ti and the decrease of Hf in the fracture coating (A1a) and the decrease of Ti in the slice adjacent to the fracture (A1b).*

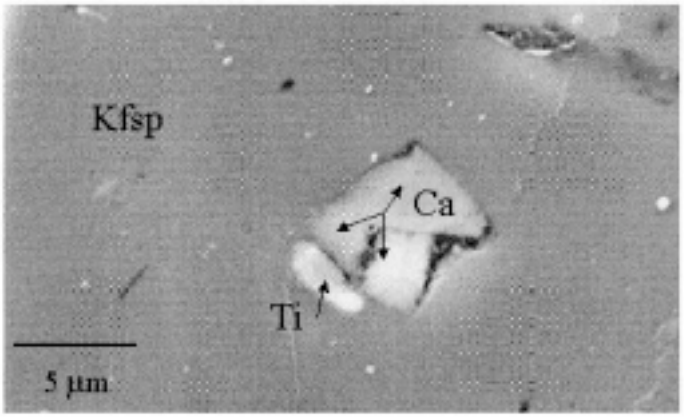

Figure 6-5. *SEM image showing Ti-oxide (Ti) and calcite (Ca) in a K-feldspar (Kfsp) crystal from the YA 1192 coating.*

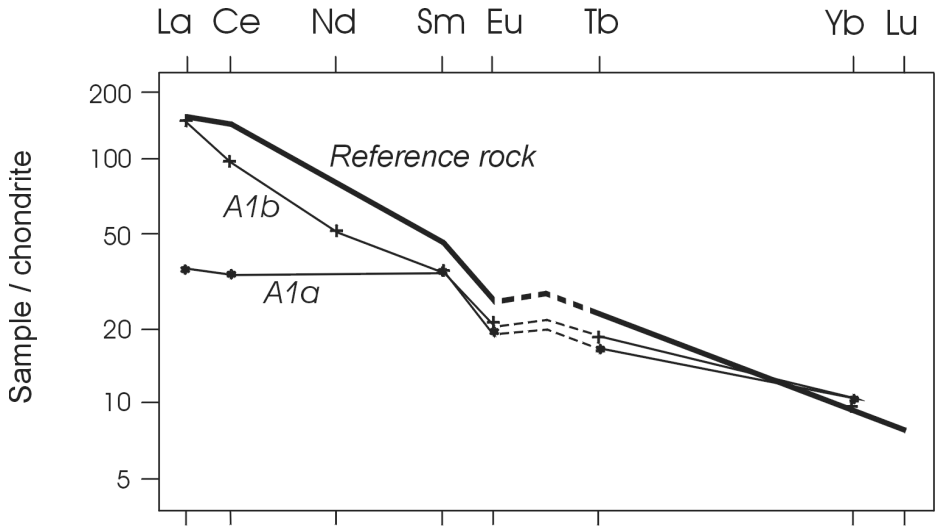

Figure 6-6. *Chondrite – normalised REE pattern for YA 1192 samples: fracture coating (A1a), slice adjacent to fracture (A1b) and reference rock.*

Fe, Co, Cr, Ni, Sc, V and Zn

The concentrations of these elements are significantly higher in the fracture coating than in the reference rock (Table 6-2). Co, Cr, Ni, Sc, V and Zn correlate with Fe in the wall rock samples, indicating coexistence in iron-bearing minerals (illustrated for V and Co in Figures 6-7a and 6-7b, respectively). Also, the fracture coating values for V, Ni and Sc fall on the regression line (illustrated for V by sample A1a in Figure 6-7a) whereas those for Co, Cr and Zn deviate from the regression line by significantly higher values (illustrated for Co by sample A1a in Figure 6-7b). It is suggested that the trace elements Co, Cr, Ni, Sc, V and Zn were mobilised in connection with alteration of iron-bearing minerals (e.g. biotite) in the outermost wall rock and generally followed Fe in the transfer to secondary minerals in the coating (e.g. chlorite). The fact that the correlation of V, Ni and Sc with Fe also includes the fracture coating values indicates that iron has not been selectively added to the coating by precipitation from fracture groundwater (see also section 7.3). The excess Cr in the fracture coating is contamination from the knife used in the sampling and the excess Co and Zn have probably been sorbed from fracture groundwater.

^{228}Th and Ra isotopes

There is a significant disequilibrium between ^{228}Th and ^{232}Th in the YA 1192 fracture coating (^{228}Th/ ^{232}Th =11.1; cf. Table 6-3). Relevant parts of the ^{232}Th decay chain are shown below:

$$^{232}\text{Th}(\alpha,1.39 \cdot 10^{10}\text{y}) \rightarrow {}^{228}\text{Ra}(\beta, 5.75\text{y}) \rightarrow {}^{228}\text{Ac}(\beta, 6.13\text{h}) \rightarrow {}^{228}\text{Th}(\alpha,1.913\text{y}).$$

The high ^{228}Th /^{232}Th activity ratio may be explained by two processes:
– Sorption of ^{228}Ra from fracture groundwater and subsequent decay to ^{228}Th.
– Sorption of ^{228}Th produced by ^{228}Ra dissolved in fracture groundwater.

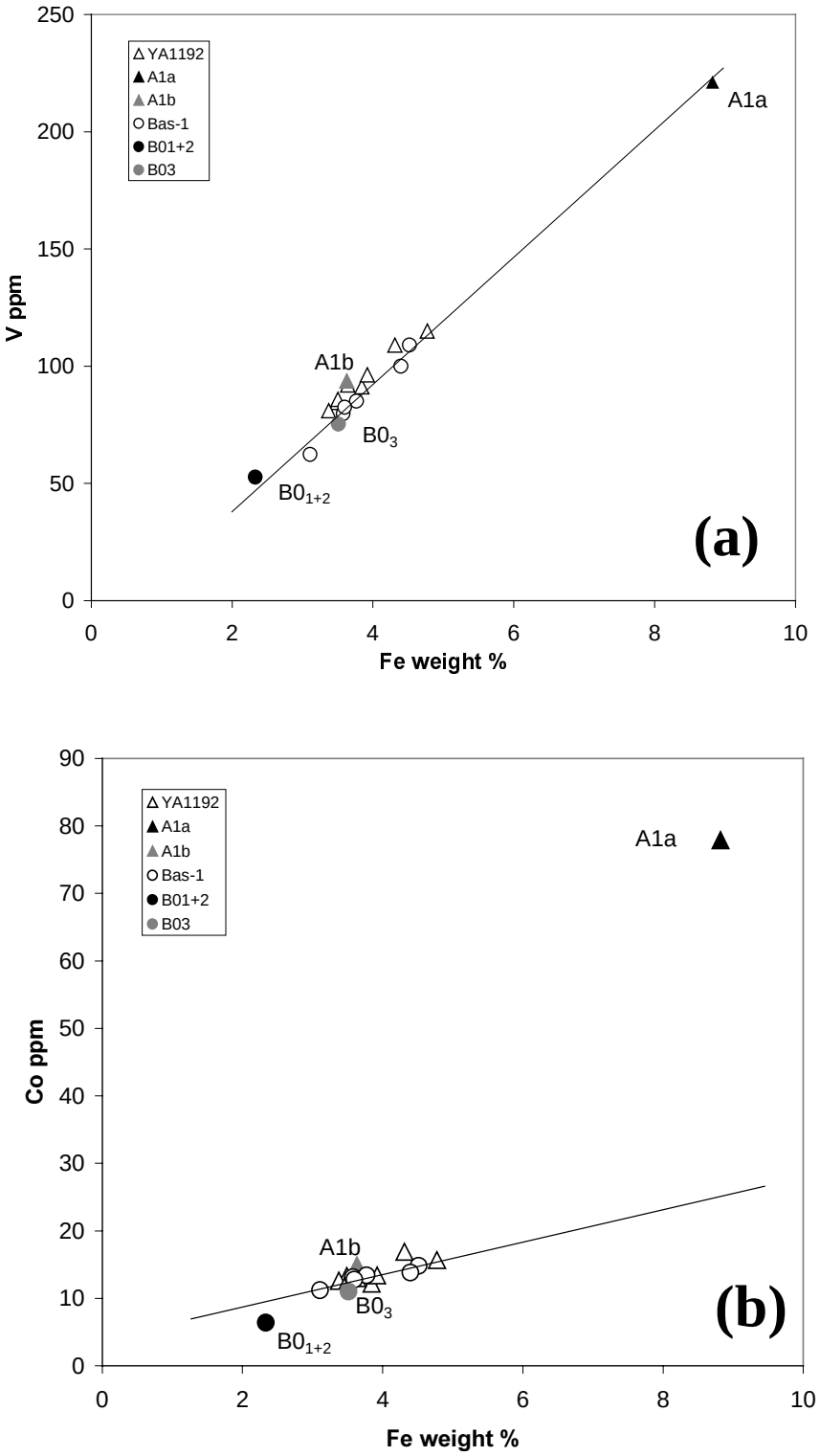

Figure 6-7.

a) Plot of V versus Fe for samples from YA 1192 and BAS 1. The regression line is calculated for the wall rock samples (i.e. excluding A1a, A1b, $B0_{1+2}$ and $B0_3$).

b) Plot of Co versus Fe for samples from YA 1192 and BAS 1. The regression line is calculated for the wall rock samples (i.e. excluding A1a, A1b, $B0_{1+2}$ and $B0_3$).

We suggest that the former process dominates. The short half-lives of the two radionuclides (^{228}Ra and ^{228}Th) imply that the sorption processes are very recent and most probably ongoing. By analogy, it is expected that also ^{226}Ra (from ^{230}Th) is sorbed onto the coating from fracture groundwater. This illustrates a probably significant source of radon in fracture groundwater since the surface sites of sorbed ^{226}Ra (progenitor of ^{222}Rn) and ^{224}Ra (daughter of ^{228}Th and progenitor of ^{220}Rn) favour recoil release of the Rn atoms to groundwater. Concentrations and distributions of ^{228}Ra and ^{226}Ra in fracture coatings and associated groundwater would be very informative about cycles of Th, Ra and Rn isotopes in fractured rocks /cf. Landström and Tullborg, 1995/. A problem is, however, the usually small fracture coating/infilling samples available, which makes the Ra analyses difficult.

6.2 Core BAS-I

6.2.1 Mineralogy and mineral alteration

The rock type at the BAS 1 site (Figure 4-1b) is a porphyritic, quartz monzodiorite-granodiorite. The matrix is medium-grained with phenocrysts of K-feldspar in the size range of 1–2 cm. The dominating minerals are plagioclase (42%) with a Na/Ca atomic ratio of approx. 3 (= oligoclase), quartz (15%) and K-feldspar (18%). The biotite has almost entirely been altered to chlorite (10%) with a Fe/Mg atomic ratio of 0.65. Other secondary minerals are epidote (5%), muscovite (1%) and fluorite (1%). The alteration processes, which have generated these secondary minerals, are not recent but associated with late magmatic or hydrothermal activity. Small amounts of hornblende are present (1%). Accessory minerals include titanite, fluorite, apatite and zircon.

Although alteration of biotite to chlorite is observed throughout the core, major element chemistry is undisturbed in large scale (except for Ca). For example, average concentrations of major elements in samples B1–B8 plot, as do those of fresh Äspö diorite, within the monzodiorite field in the R1–R2 classification diagram /de la Roche et al., 1980/. Also, the trace element concentrations generally agree with those of fresh Äspö diorite. However, small-scale redistribution of major and trace elements between different minerals have most probably occurred. This is apparent in the secondary mineral fluorite, formed from fluorine mobilised in connection with breakdown of biotite.

A relatively thin (0.2–0.5 cm thick) weathered rim appears in the surface of the BAS 1 outcrop. Microscopy and SEM images of the rim show that quartz and K-feldspar have remained almost unaltered whereas alteration of plagioclase and chlorite has created uneven, “bumpy” surfaces (Figure 6-8). A closer examination revealed small remnants of intact plagioclase surrounded by weathering products, which had significantly higher Al_2O_3/SiO_2, Na_2O/CaO and Al_2O_3/Na_2O ratios, higher porosity and higher water content than unweathered plagioclase. These ratios of the weathered products are similar to those of clay minerals and consistent with the loss of SiO_2, CaO and Na_2O relative to K_2O in the weathered surface sample (Table 6-4).

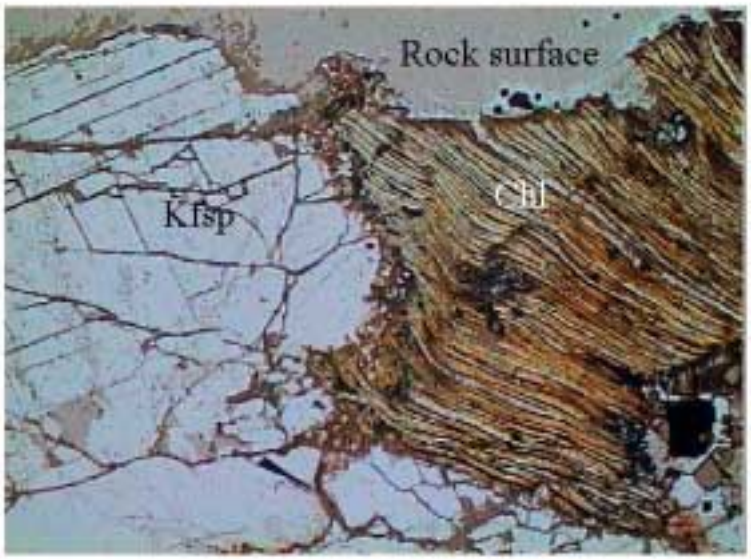

Figure 6-8. *Photomicrograph showing chlorite (Chl) and K-feldspar (Kfsp) close to the surface in BAS 1. Length of the photo corresponds to 2.5 mm.*

SEM/EDS studies of weathered chlorite from the surface rim show that this chlorite has a lower content of MnO and MgO+FeO and a slightly lower Al_2O_3/SiO_2 ratio than unweathered chlorite. However, whole-rock analysis of the weathered surface rim (sample $B0_{1+2}$, Table 6-4) shows much lower MgO than can be explained by alteration of chlorite alone. It is then suggested that part of the chlorite has been entirely removed from the surface through chemical dissolution and/or physical weathering.

From laboratory experiments Malmström et al. /1995/ reported that the dissolution of chlorite was more stoichiometric than the dissolution of biotite; no real alteration products were identified and no significant changes in FeII/FeIII were observed. This supports the above interpretation that chlorite in the BAS 1 surface has been dissolved rather than altered. SEM images show that the weathering has followed the layer structure of the chlorite and extended the distance between the layers. This has resulted in increased exposure to physical weathering processes; for example frost shattering. Accessory minerals such as zircon and apatite are usually embedded in the chlorite and can thus be released in association with the dissolution/alteration of chlorite.

Pyrite is found in spots as small accessory grains. SEM analysis of two pyrite grains in the weathered surface rim (located 0.5 and 1 mm, respectively, from the surface) shows oxidation, visualised as cores of pyrite surrounded by FeOOH (Figure 6-9). Note that the outermost pyrite grain (with a smaller pyrite core) is significantly more oxidised. In contrast, a pyrite grain located 15 mm from the surface, shows no signs of oxidation (Figure 6-9).

Table 6-4. Major (in %) and trace element (in ppm) concentrations for samples from the BAS 1 core. Sample $B0_{1+2}$ represents the weathered surface rim and sample ($B0_3$) the upper slice.

Element	B01+2	B03	B1	B2	B3	B4	B6	B8	%loss*
$Si0_2$ %	64.0	61.9	59.8	62.2	60.4	60.3	58.8	61.1	35.5
Al_2O_3	17.0	18.0	17.6	17.9	17.1	17.2	17.3	17.0	38.1
CaO	2.43	3.44	3.4	3.34	4.01	4.27	4.65	4.44	63.2
Fe_2O_3	3.33	5.02	5.11	4.44	6.45	5.39	6.28	5.14	63.0
K_2O	4.29	2.52	3.53	3.48	2.68	2.35	1.83	1.81	0
MgO	1.24	2.82	2.64	2.52	2.99	2.72	2.97	2.64	72.6
MnO	0.056	0.089	0.097	0.087	0.102	0.095	0.105	0.094	64.9
Na_2O	4.2	4.71	4.08	4.43	4.04	4.43	4.7	4.61	41.7
P_2O_5	0.235	0.334	0.335	0.325	0.394	0.365	0.365	0.335	59.5
TiO_2	0.718	0.768	0.824	0.748	0.933	0.917	0.968	0.901	50.5
LOI	2.2	1.7	1.5	1.4	1.5	1.5	1.4	1.4	
Rb ppm	141	83.4	110	83.3	93	87.9	78	68	1.1
Cs	2.09	1.85	1.94	1.75	2.19	2.44	2.47	2.3	41.7
Be	2.76	3.53	3.14	3.08	3.73	3.76	4.13	3.87	53.6
Sr	1150	1160	1120	1160	1090	1130	1140	1130	38.1
Ba	2340	1190	2340	1490	1570	1440	787	790	7.7
V	52.7	75.2	79.7	62.3	109	85.1	100	82.4	62.9
Cr	55.6	51.1	48.6	32.3	56.4	37.8	46.1	32	19.8
Co	6.4	11.0	13.1	11.2	14.8	13.4	13.8	12.8	70.5
Ni	24.1	26.9	32.5	22.7	33.3	27.1	30.5	27.6	49.4
Cu	50.3	77.7	59.0	54.3	66.8	53.4	14.5	26.5	35.5
Zn	55.3	78.6	82	80	102	102	92	80	62.5
Zr	274	256	255	234	310	317	320	378	44.8
Hf	5.83	6.54	7.54	5.71	7.85	8.5	7.76	7.71	52.5
Nb	<12	<12	<12	<12	15.8	14.2	15.8	16.7	–
Ta	1.19	1.0	1.35	0.82	1.31	1.35	1.21	1.42	41.6
Th	10.4	10.4	13.5	10.3	14.2	17.6	13.2	12.7	53.5
U	2.97	3.5	3.5	3.0	4.83	4.35	5.1	4.87	58
Sc	6.44	8.85	11.2	9.72	10.4	8.49	10.9	9.28	60.8
La	36.1	49.1	61.8	45.6	67.1	66.0	53.5	61.0	62.9
Ce	88	103	136	93.8	137	139	113	131	57.2
Nd	40	45.8	63	40.7	58	59	55	60	56.5
Sm	7.21	7.5	10.4	6.48	9.9	10.5	8.74	10.8	53.7
Eu	1.45	1.62	2.16	1.39	2.00	2.00	1.94	2.07	54.3
Tb	0.87	0.91	1.3	0.81	1.2	1.18	0.98	1.24	52.7
Yb	1.74	1.8	2.65	1.69	2.43	2.51	2.25	2.49	54.8
Lu	0.25	0.28	0.39	0.28	0.38	0.39	0.34	0.39	57.8
Y	16.3	16.0	21.9	16.6	22.9	23.2	24.2	24.8	55.5

* The percentage loss from the weathered surface rim has been related to the concentration of K and to the host rock composition (average of samples B1 to B8).

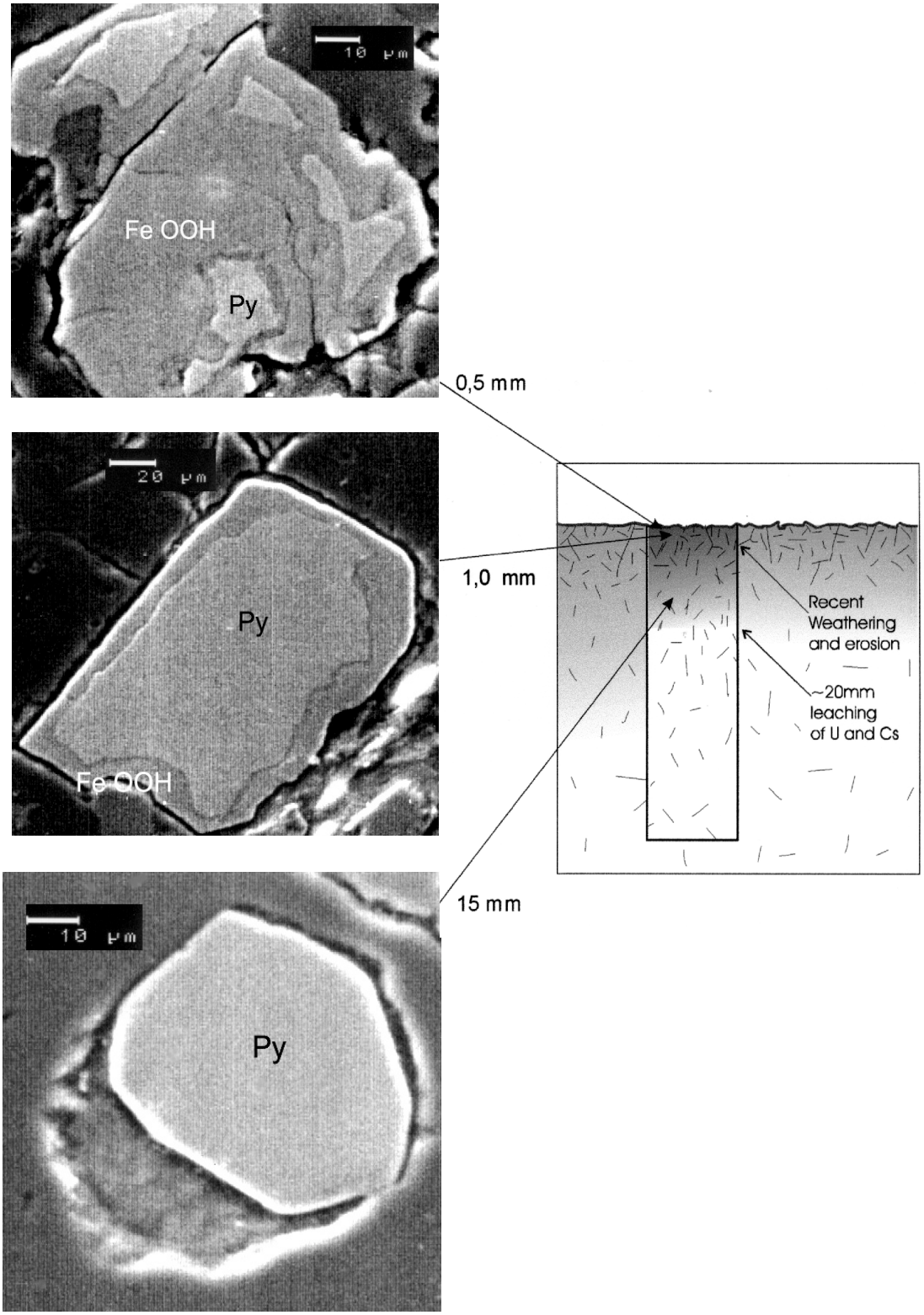

Figure 6-9. *SEM images showing pyrite grains in different stages of oxidation close to the outcrop surface at Bas-1 and unaltered pyrite at 15 mm depth.*

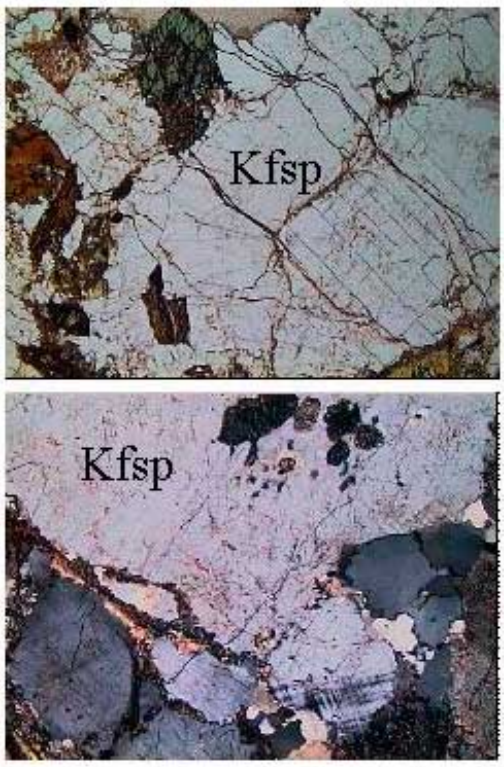

Figure 6-10. *Micro fractures in K-feldspar (Kfsp) close to the surface (upper: parallel nicols) and 20 mm from the surface (lower: crossed nicols). Length of photomicrographs corresponds to 2.5 mm.*

Porosity measurements on two samples, approx. 10 and 20 cm, respectively, below the bedrock surface, show values of ≈ 0.5 volume %; i.e. slightly higher than that of fresh Äspö diorite (≈ 0.4 volume %) and presumably attributed to the post-magmatic alteration. No porosity measurements were carried out in the upper part of the core. However, besides the obviously high porosity in the weathered surface rim (Figure 6-8), microscopy shows an increased frequency of microfractures (especially in the K-feldspar and quartz grains) in the upper 1–2 cm of the BAS 1 core suggesting that the porosity increases towards the surface (Figure 6-10). The latter is supported by results from impregnation studies (14C-PMMA) of porosity in a core drilled from a granite outcrop at Palmottu, southern Finland /Siitari-Kauppi et al., 1999/. Values of 6 volume % at the surface, 1 volume % at 1 cm depth and 0.4 volume % at 3 cm depth were obtained. Since this outcrop probably has been exposed to glacial/post-glacial weathering, corresponding to that at the BAS 1 site, a similar porosity trend may be expected for the BAS 1 outcrop.

6.2.2 Geochemistry

General

Concentrations of major and trace elements and loss on ignition (LOI) values are presented in Table 6-4 and activity ratios of U and Th isotopes in Table 6-5. Averages of element concentrations for samples B1 to B8 are assumed to represent the host rock composition, and referred to as "host rock". The medium-grained rock (with phenocrysts of K-feldspar as large as 1–2 cm) and the small volume of the slices make a representative sampling difficult. Variations in trace (and major) elements may thus be due to textural variations rather than to, for example, alteration or matrix diffusion effects.

Table 6-5. Concentrations of Th and U (alpha-spectrometry) and activity ratios for the Bas 1 core.

Sample number	Th (ppm) alpha-sp.	U (ppm) alpha-sp.	$^{234}U/^{238}U$	$^{230}Th/^{234}U$
$B0_{1+2}$	15.8	3.8	0.96	1.53
$B0_{3}$	13.5	4.7	1.0	1.37
B1	16.5	4.4	0.91	1.85
B2	15.5	5.1	0.92	1.52
B4	23.2	6.5	0.95	1.16

The following description of the geochemistry is focused on i) weathering effects in the thin surface rim, ii) indications of leaching/diffusion in the 2 cm zone below the exposed surface, and iii) indications of redox conditions.

Weathering effects in the surface rim

The most conspicuous weathering in the glacial-polished surface at BAS 1 is suggested to be dominantly post-glacial (i.e. has operated on the uncovered rock surface during the last 4 ka) and has resulted in a 0.2–0.5 cm thick weathered rim. It involves both chemical alteration and mechanical erosion caused by, for example, freeze and thaw reactions. For example, dissolution of chlorite and plagioclase occurs as well as particulate release of resistant minerals embedded in the chlorite (e.g. zircon). The exposed surface is characterised by "remnants" of K-feldspar and quartz.

Relative to host rock, only Si, K, Ba and Rb show higher concentrations in the weathered surface rim (represented by sample $B0_{1+2}$; Table 6-4). All other elements are lower than, or similar to the host rock values. This is consistent with the results of thin section studies; i.e. that quartz and K-feldspar (predominantly hosting K, Ba and Rb) have been unaffected by the post-glacial chemical weathering. However, some fragments of K-feldspar may have been removed by physical weathering.

Conservative elements (Ti, Zr and Hf) and mass balance calculations

The Ti/K, Zr/K and Hf/K ratios for the weathered surface rim (sample $B0_{1+2}$) are only half of those for the host rock. This indicates a substantial loss of Ti, Zr and Hf, relative to K. The host minerals of these elements (e.g. titanite, ilmenite and rutile for Ti, and zircon for Zr and Hf) are usually embedded in chlorite, and probably liberated in connection with dissolution/alteration of this mineral. Since zircon is very resistant to chemical weathering, Zr and Hf have been released and transported in particulate form. This is probably also the case of Ti, although post-glacial weathering of titanite in soil has been reported /Lång, 2000/. Neither Ti nor Zr and Hf can thus be used as immobile conservative elements in estimation of element loss. Instead, the percentage loss from the weathered surface rim has been related to the concentration of K and to the host rock composition (average of samples B1 to B8). The latter is assumed to represent the original composition of the weathered rim. Values of percentage loss, relative to K, is given in Table 6-4.

Ca, Mg, P, Na, Sr and Cs

Relative to K, 63, 60 and 72%, respectively, of Ca, P and Mg have been lost from the weathered rim (Table 6-4), reflecting mechanical erosion and/or chemical dissolution of plagioclace, apatite, possibly epidote and accessory calcite (Ca and P) and chlorite (Mg). The percentage loss of Na is lower (42%) demonstrating the higher resistance to weathering of albite components in the plagioclase. The percentage loss of Sr and Cs are similar to those of Na (38 and 42%, respectively).

U, Th, REEs and Y

The percentage loss of U, Th, REEs and Y, relative to K, are similar to or slightly higher than that of Hf (Table 6-4) and probably due to physical weathering, i.e. transportation in mineral particles. However, U occasionally occurs at grain boundaries that are easily attacked by the fluid phase when the mineral structures are opened through physical weathering. A small fraction of U may thus have been leached and transported in solution. The chondrite-normalised REE pattern of the weathered surface rim (sample $B0_{1+2}$ in Figure 6-11) indicates a slight fractionation in light REEs, relative to host rock.

Fe, Co, Cr, Ni, Sc, V and Zn

The trace elements Co, Cr, Ni, Sc, V and Zn correlate with Fe in the rock samples indicating co-existence in iron-bearing minerals (illustrated for V and Co in Figures 6-7a and 6-7b, respectively). The percentage loss of Co, Sc, V and Zn from the weathered surface rim (sample $B0_{1+2}$) are close to that of Fe, suggesting similar behaviour (Table 6-4). Physical erosion of iron-bearing minerals is probably the dominant mechanism for the loss of these elements. Contamination by the metal chisel has caused the seemingly low percentage loss of Cr (and possibly also of Ni).

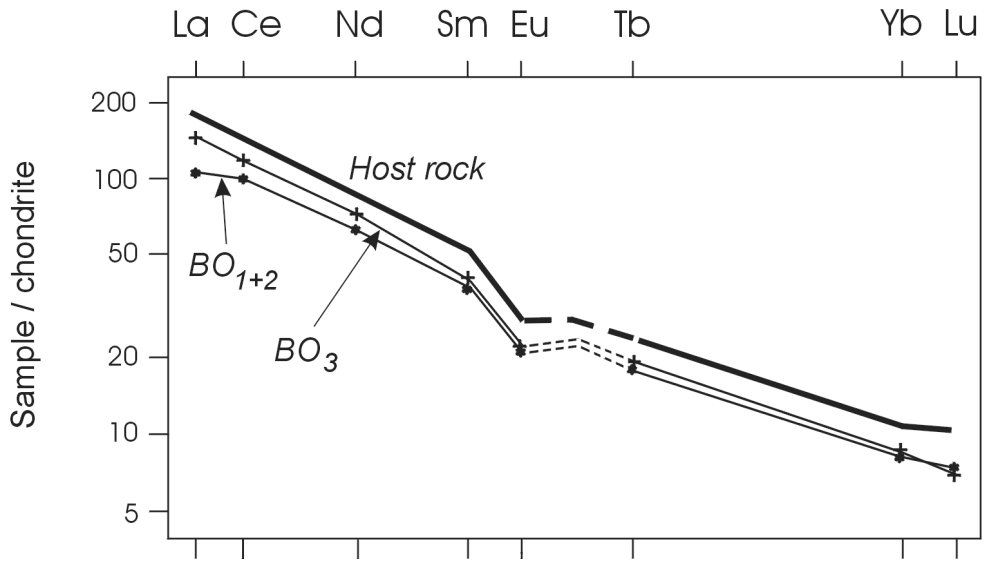

Figure 6-11. *Chondrite normalised REE pattern for BAS 1 samples: weathered surface rim ($B0_{1+2}$.), upper slice ($B0_3$) and host rock.*

Extent of the post-glacial surface weathering, based on mineralogical and geochemical results

Applying results from studies on dissolution of chlorite /Malmström et al., 1995/, it is estimated that the amount of chlorite dissolved during the 4–5 ka period Äspö has been above sea level, corresponds to < 0.1 mm of the bedrock. However, chemical analyses from the BAS-1 core indicate a much higher loss of chlorite, corresponding to a 1–2 mm thick zone. This suggests that mechanical erosion significantly dominates over chemical alteration/dissolution. Also, the large loss of the resistant zircon indicates physical weathering to be more active than chemical weathering. The percentage loss of Zr and Hf, relative to K, is in average 50% and may be a rough measure of percentage elemental loss due to erosion and particulate transportation. The percentage loss exceeding this value may then indicate the fraction of elemental loss due to chemical weathering and transport in solution. However, as zircons are frequently embedded in chlorite, the preferential weathering and breakdown of chlorite (see above) may favour the physical release of zircons relative to other minerals.

An estimation of the total material eroded from the exposed surface is difficult. The general opinion /e.g. Swantesson 1992 and references therein/ is that the post-glacial erosion of the crystalline bedrock in Sweden is in the order of mm to one centimetre. The presence of well-preserved striations in the Äspö area indicates that post-glacial erosion has not exceeded 1–2 cm.

The percentage loss values in Table 6-4 cluster in different groups. From the combination of elements in a group one may disclose which minerals have been dissolved and/or eroded. This allows a rough ranking (in decreasing order) of the minerals in the outcropping granodiorite with respect to their resistance to this type of post-glacial erosion and chemical weathering: K-feldspar (K, Ba and Rb, 0–7%), albite (Na, Sr, 38–41%), zircon (Zr and Hf, 45–52%), titanite, ilmenite (Ti, 51%), accessory REE-bearing minerals (REEs, 55–63%), plagioclase, epidote and apatite, (Ca and P, 60–63%), chlorite, hornblende, (Fe, Mn, V, Zn, 63–65% and Mg, 72%).

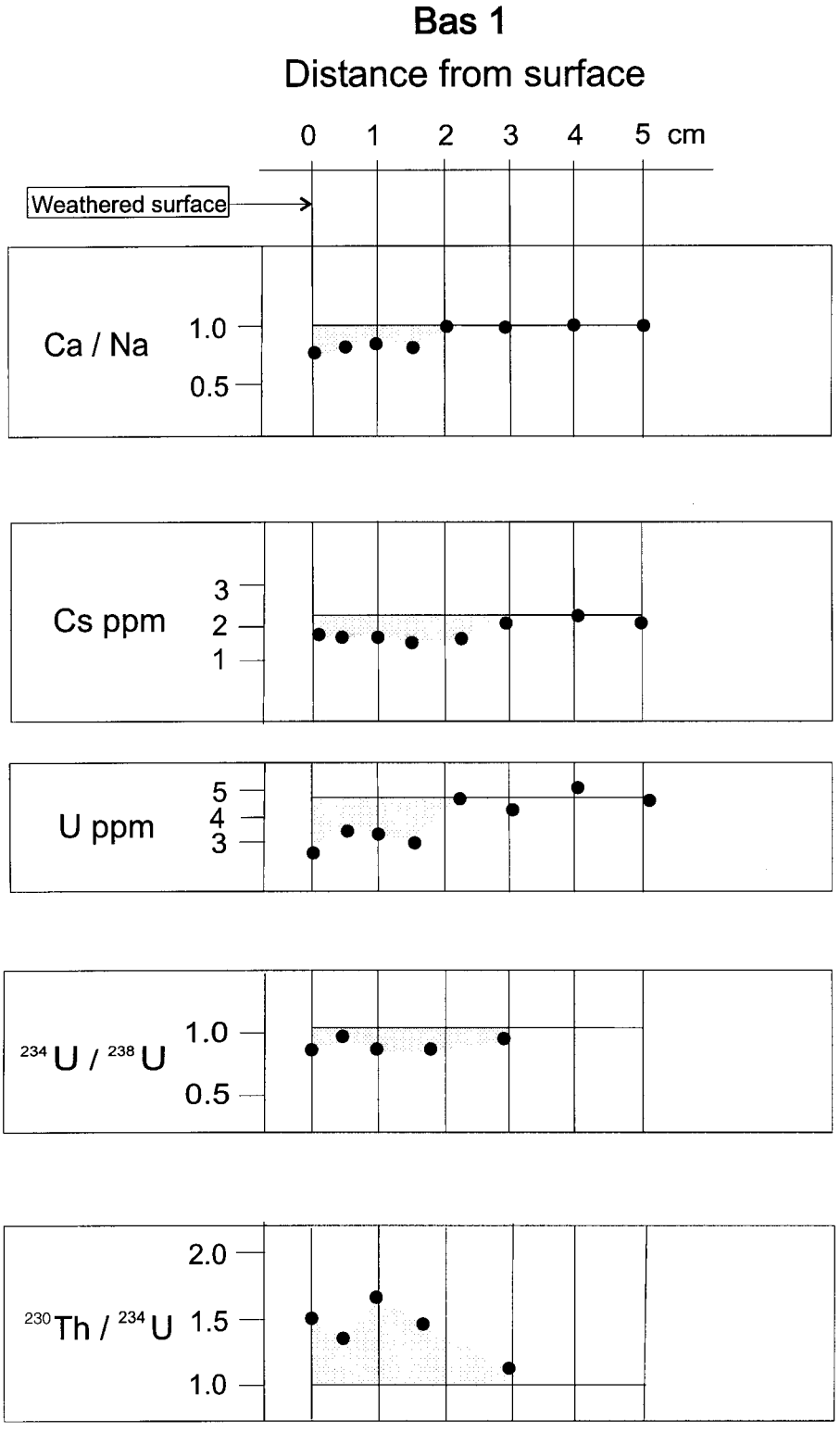

Figure 6-12. *Depth profiles of Ca/Na ratio, Cs, U, $^{234}U/^{238}U$ and $^{230}Th/^{234}U$ activity ratios in core BAS 1. The reference levels are average values of samples B1 to B8 (assumed to be representative of unaltered host rock).*

Indications of leaching/diffusion in a 2-cm zone below the surface

Besides the distinct weathering in the BAS 1 surface (described in section 6.2.2 – Weathering effects in the surface rim), water/rock interactions are indicated in a 2-cm zone below the exposed surface; by decrease in the Ca/Na ratio and in the Cs and U concentrations (Figure 6-12). Although textural variations may in part explain the negative Ca/Na, Cs and U anomalies in Figure 6-12, it is suggested that significant leaching of Ca, Cs and U has occurred. This is consistent with the increased frequency of microfractures close to the BAS 1 surface (Figure 6-10), giving access to migration pathways for the mobilised elements. The decrease in the Ca/Na ratio implies preferential leaching of Ca, relative to Na, possibly the result of slight alteration of plagioclase. Leaching of Cs seems to be favoured by the BAS 1 mineralogy and is supported by the Cs/K ratio profile in Figure 7-1 (c.f. discussion in section 7.2).

The $^{234}U/^{238}U$ activity ratios are close to or slightly below unity whereas the $^{230}Th/^{234}U$ activity ratios significantly exceed unity (Table 6-5 and Figure 6-12). This indicates "congruent" or "bulk" leaching (i.e. with insignificant fractionation of U isotopes) within the last 0.35 Ma. However, the leaching of U (and Cs as well) is assumed to be associated with the late Weichselian glaciation, (i.e. confined to the last 100 ka) since weathering zones from earlier glaciations have most probably been eroded. As discussed in section 7.2, this interpretation is supported by results from studies of Suksi and Rasilainen /2000/ and Gascoyne and Cramer /1987/.

Indications of redox conditions

– The alteration of pyrite in the uppermost mm of the BAS 1 surface (see Figure 6-9) is interpreted as the result of oxidising groundwater penetration (glacial melt water and/or later meteoric). The pyrite grains found in the upper 2 mm exhibit a decreasing degree of alteration; the outermost grain shows only a small core of pyrite surrounded by FeOOH whereas the innermost grain shows only a thin rim of FeOOH. In contrast, pyrite grains at 12–15 mm are totally fresh.

– U bulk leaching as the result of oxidative leaching (with $^{234}U/^{238}U \cong 1$) has occurred in the upper 20 mm of the bedrock surface within the last glacial/post-glacial period (cf. section 7.2).

It should be noted that the depths of oxidation described by the two indicators do not correspond since oxidation of pyrite is only seen in grains located within upper millimetres of the surface whereas the oxidative leaching of U is traced to 20 mm depth. Alternative explanations are discussed in section 7.3.

7 Discussion

7.1 General

When discussing and comparing the results from the two cores one should be reminded that the rocks are medium-grained, the analysed volumes relatively small, the distance between the core sites about 1 km and the location of the YA 1192 core is 170 m below the bedrock surface. The fracture surface of the YA 1192 core has probably been in contact with groundwater during long periods of time, in hydrothermal as well as in low-temperature regimes. Mineral/water reactions have affected a narrow (2–3 cm) zone of the wall rock adjacent to the fracture and have formed coatings on the fracture wall, with chemical and mineralogical compositions that strongly differ from those of the wall rock.

In contrast, the bedrock surface at BAS 1 was intensely worked by the ice during the late Weichselian glaciation, covered by till and Baltic sediments after deglaciation and exposed to air, precipitation and snow cover during the last 4–5 ka. Pre-quaternary weathered zones as well as weathered zones from earlier quaternary glaciations have been removed. The weathering effects now observed in the BAS 1 core (a thin weathered surface rim and depletion of Ca, U and Cs in a 2-cm zone below the surface) are thus most probably confined to the late glacial/post-glacial period.

Comparison of the YA 1192 reference rock (average of samples A8, A10 and A13 in Table 6-2) and the BAS 1 host rock (average of samples B1 to B8 in Table 6-4) shows that the concentrations of most major and trace elements are similar at the two sites. However, BAS 1 differs from YA 1192 in lower concentrations of K, Ba and Cu (approx. 20, 30 and 50%, respectively) and in higher concentrations of Mg (20%), Zr and Hf (30%), Ta, Zn, Th and U (60 to 80%). This may be related to the post-magmatic alteration (visible as chloritisation in the Bas 1 core) and circulation of late magmatic fluids causing enrichment of incompatible elements in BAS 1, such as Zr, Hf, Ta, U and Th.

7.2 Evidences of matrix diffusion – comparison with other sites

Conditions which facilitate retardation through diffusion + sorption processes are demonstrated in the 0–3 cm zone adjacent to fracture YA 1192; increased porosity, presence of sorbing secondary minerals and saline water in connected pores and micro-fractures. The excess ^{234}U and the increase in Cs in the same zone (Figure 6-3) are then consistent with in-diffusion of U and Cs from fracture groundwater, and subsequent sorption onto secondary minerals. There are no indications of alternative origins for U and Cs, e.g. from deeper parts of the wall rock. The excess ^{234}U implies deposition of U within the last 1 Ma.

Similar results were obtained in analyses of a drill-core crosscutting a water-conducting fracture at 317 m depth in the nearby Götemar granite; $^{234}U/^{238}U > 1$ and increase in Cs relative to host rock in the 0–3 cm zone adjacent to the fracture /Smellie et al., 1986 and

discussed in Alexander et al., 1990/. The uranium data were interpreted as recent (< 1 Ma) deposition of U and that at least part of the U originated in fracture groundwater; i.e. by processes similar to those suggested for YA 1192. In a corresponding study from the Kamaishi site in Japan, Ota et al. /1997/ report on a hydrothermally altered zone adjacent to a water-conducting fracture, extending 5 cm into the granodioritic wall rock. The zone is characterised by connected porosity, decreasing with distance from the fracture. They interpreted the increase in U, $^{234}U/^{238}U$ activity ratios > 1 and $^{230}Th/^{234}U$ activity ratios < 1 as diffusion of U into the altered zone, occurring within the last 300 ka. A correspondence between the extent of alteration zones adjacent to water conducting fractures and in-diffusion of U, evidenced by uranium series measurements, has also been reported from several other sites e.g. Böttstein and Grimsel in Switzerland /Smellie et al., 1986/, El Berrocal in Spain /Heath and Montoto, 1996/ and Eye-Dashwa Lakes granite pluton in Canada /Gascoyne and Schwarcz, 1986/. Miller et al. /1994/ conclude in their review that; "Comprehensive geochemical and petrophysical characterisation reveals that the region of enhanced trace element mobility in the vicinity of a fracture often corresponds to zones of physical or hydrothermal alteration".

The studies cited above support the conception of matrix diffusion as a retardation mechanism for uranium. They also emphasise that alteration processes in the rock adjacent to fractures are, if not a prerequisite, crucial in creating conditions favourable to matrix diffusion; e.g., increased porosity and sorbing secondary minerals. The common depth of about 2–5 cm for such alteration zones as well as for observed disequilibria in the ^{238}U decay chain probably is a realistic range of matrix diffusion of radionuclides with half-lives typical of those in HLW.

While a diffusion media is clearly recognised in the hydrothermally altered zone at YA 1192 (see above), this is not so evident concerning the BAS 1 core. However, increase in porosity towards the fracture is examined by microscopy that also links the porosity to increased frequency of microfractures (see section 6.2.1 and Figure 6-10). Moreover, the decrease in the Ca/Na ratio in the 2-cm zone below the exposed surface (Figure 6-12) indicates loss of Ca, in preference to Na, probably the result of alteration of plagioclase (see section 6.2.1). The depletion of Cs and U relative to host rock (Figure 6-12) is then consistent with leaching/diffusion processes. The $^{234}U/^{238}U$ and $^{230}Th/^{234}U$ activity ratios and geological data, indicate bulk leaching of U within the last 100 ka (c.f. section 6.2.2 – Indications of leaching/diffusion in a 2-cm zone below the surface).

The interpretation of the uranium and thorium data for BAS 1 is supported by results from studies of Suksi and Rasilainen /2000/ and Gascoyne and Cramer /1987/. Suksi and Rasilainen analysed core slices, sampled perpendicular to fractures in the upper bedrock at Palmottu (from 31.5 and 34 m depth). Typical results were $^{234}U/^{238}U \cong 1$ for slices adjacent to fractures, which carried oxidising groundwater, but $^{234}U/^{238}U < 1$ farther away from the fracture, at the redox front. These data were explained as being effects of "recoil induced oxidation" of ^{234}U; i.e. ^{234}U is oxidised to the "mobile" $^{234}U(VI)$ when formed by decay of the recoiled ^{234}Th (via ^{234}Pa). In a reducing environment (e.g. at the redox front) $^{234}U(VI)$ is leached in preference to $^{238}U(IV)$ resulting in $^{234}U/^{238}U$ ratios < 1 for the solid phase. In an oxidising environment (e.g. close to the fracture) also $^{238}U(IV)$ is oxidised, to the "mobile" $^{238}U(VI)$, resulting in congruent leaching and $^{234}U/^{238}U \cong 1$ for the solid phase. The $^{230}Th/^{234}U$ activity ratios, associated with the congruent leaching, exceeded unity, indicating that the congruent leaching of U occurred within the last 0.35 Ma. Similar results were obtained in analyses of a core from the surface of the Lac de Bonnet granite: $^{234}U/^{238}U \cong 1$ and $^{230}Th/^{234}U > 1$ /Gascoyne and

Cramer, 1987/. These data were interpreted as bulk leaching of U within the last 350 ka, and probably within the last 100 ka.

Referring to the studies at the Palmottu, Lac de Bonnet and Äspö sites, all being situated in glaciated areas, bulk leaching of U within the last 350 ka and under oxidising conditions may be a widespread event in the upper part of crystalline rocks exposed to glaciation. Since the 350 ka period coincides with at least two glaciations, a central question is whether glacial meltwater during glaciations/deglaciations or meteoric water during interstadial/interglacial periods has dominated the oxidative leaching of U. This is discussed for BAS 1 in section 7.3.

Concerning interpretations of the Cs anomalies (cf. Figures 6-3 and 6-12), some differences in mineralogy between the cores should be noticed. While biotite is altered to chlorite throughout the BAS 1 core, it is preserved in the YA 1192 core and sericite has formed by alteration of plagioclase. Both biotite and sericite have high sorption capacity for Cs, thus favouring sorption of Cs in YA 1192. By contrast, these minerals occur in very minor amounts in the BAS 1 core. Moreover, the Cs contained in the altered biotite was probably transferred to sites in chlorite, comparatively accessible to leaching, or sorbed on other mineral phases (mobilisation of this Cs is not indicated by, for example, lower Cs concentration in BAS 1 host rock relative to YA 1192 reference rock). The differences in mineralogy between YA 1192 and BAS 1 may thus have contributed to the formation of the Cs anomalies, by favouring sorption in YA 1192 and leaching in BAS 1, respectively.

The conceptions of Cs deposition in YA 1192 and Cs leaching in BAS 1 (see Figures 6-3 and 6-12) are supported by the Cs/K ratio profiles in Figure 7-1. Cs and K usually coexist in primary minerals; in these rocks mainly in biotite and K-feldspar (with Cs/K ratios typically in the order of $1.2 \cdot 10^{-4}$ and $0.2 \cdot 10^{-4}$, respectively). The mirror image of the Cs/K ratio profiles in Figure 7-1 indicates migration of Cs in preference to K. Although not illustrated, the Cs/Rb ratio shows the same trend as the Cs/K ratio.

In conclusion, retardation of U and Cs by matrix diffusion is indicated in the YA 1192 core. The diffusion is restricted to the hydrothermally altered zone, about 3 cm thick. Such zones usually enclose water-conducting fractures in crystalline rocks and probably set a limit for matrix diffusion retardation of waste radionuclides. Knowledge of depth and extension, porosity, distribution of microfractures and of sorbing secondary phases for such zones is important to the modelling of matrix diffusion retardation. In contrast, leaching of U and Cs (by diffusion processes) is indicated in the BAS 1 core. Bulk leaching ($^{234}U/^{238}U \cong 1$) during the last glacial/post-glacial period may have been a characteristic event in the oxic environment of surface rocks.

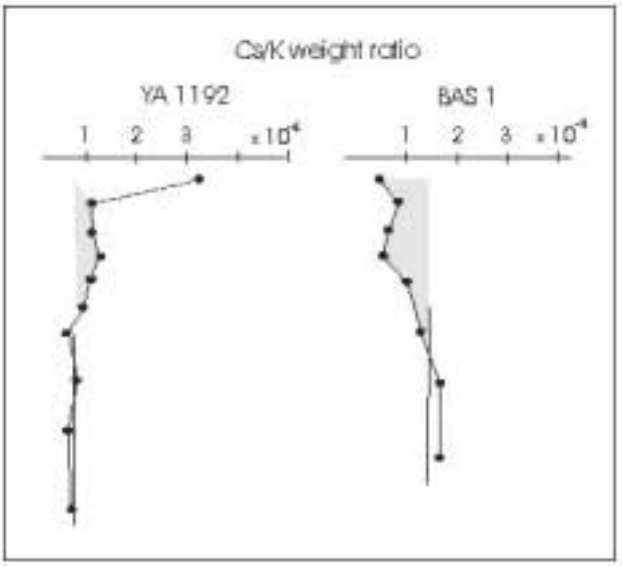

Figure 7-1. *Cs/K ratio profiles in YA 1192 and BAS 1. Cs and K usually coexist in primary minerals; in the present rocks, mainly in biotite and K-feldspar (with Cs/K ratios typically in the order of 1.2 10^{-4} and 0.2 10^{-4}, respectively). Transfer of Cs to chlorite and mobilisation of K in connection with alteration of biotite to chlorite in BAS 1 probably caused the difference in the Cs/K background values (1.4 · 10^{-4} for BAS 1 and 0.9 · 10^{-4} for YA 1192). The mirror image of the profiles indicates migration of Cs in preference to K, by diffusion processes.*

7.3 Possible influence of glacial meltwater on the redox conditions at the BAS 1 and YA 1192 sites

Models of future climate change /e.g. Imbrie and Imbrie, 1980; Berger and Loutre, 1997/ suggest that Scandinavia will be exposed to glaciations during the next 100 ka, i.e. within the time scale of concern for performance assessment of deep repositories for spent fuel. The hydrogeological and hydrochemical conditions in the bedrock probably change radically during a glacial cycle; for example, loading/unloading of ice sheets may reduce or enlarge fracture apertures and reactivate sealed fractures, permafrost may seal aquifers and glacial meltwater may infiltrate the bedrock. Such meltwater is expected to be enriched in oxygen and depleted in organics and dissolved solids and thus has potential to change the hydrochemistry, e.g. the redox conditions.

In modelling the effects of future glaciations on deep repositories, King-Clayton et al. /1995/ and Glynn et al. /1999/ predict that oxygenated glacial meltwater may reach repository levels, modify the redox conditions and thus hazard the stability of an underground repository. However, Gascoyne /1999/ has questioned these results arguing that their basic assumptions are too conservative and in part unrealistic. Moreover, Guimerà et al. /1999/ have analysed the potential advance of an oxidation front as a result of meltwater infiltration and conclude that ice melting poses no danger to the stability of a repository at 500 m depth except when the flow rate is around 10^{-5} m/s or higher. For validation, it is thus important to identify infiltration depths of glacial meltwater as well as changes in redox conditions, related to such meltwater infiltration.

Glacial meltwater is characterised by extremely low $\delta^{18}O$ and δD values. Components of groundwater with such isotope signatures have been found at depths from 134 to 450 m at Äspö ($\delta^{18}O$ values varying from –15.8 to –13.6 per mil; Laaksoharju et al., 1999). This water is now reducing and to document whether it brought oxygen into the bedrock aquifer or not is a difficult task. The oxygen contained in meltwater is consumed mainly by dissolution of Fe(II)-containing minerals (e.g. pyrite, magnetite, biotite and chlorite), resulting in formation of Fe-oxyhydroxide, but also in microbe mediated reactions with reducing gases like CH_4 and H_2 /Puigdomenech et al., 2001/. This means that the relative decrease in (or absence of) minerals like pyrite, magnetite, biotite and chlorite along the flow paths and the associated increase in Fe-oxyhydroxide may be indications of past interactions with oxygenated meltwater.

The outcropping surface at BAS 1 certainly was in contact with the ice base during the last glaciation and thus with glacial meltwater. Since zones of erosion/weathering from previous glacial cycles have been entirely eroded, two generations of "weathering" can be distinguished at BAS 1. The older one is confined to the late Weichselian glaciation and clearly includes abrasion by the moving ice sheet (remains of this abrasion are striations in the present bedrock surface) and probably also chemical interactions with glacial meltwater. The younger one is post-glacial, i.e. started operation when the BAS 1 surface was uncovered in connection with crustal uplift. Remnants of this, dominantly physical, post-glacial weathering is a thin, < 0.5 cm, surface rim. Interaction between the bedrock and pore water in the over-lying Baltic sediments may have occurred, but has not been possible to document.

The chemical weathering in the BAS 1 core is visualised as dissolution of chlorite and plagioclase in the weathered surface rim, alteration of pyrite and formation of FeOOH in the uppermost millimetres of this weathered rim, and leaching of Ca, U and Cs in the 2-cm zone below the exposed surface. Since the alteration of pyrite and the bulk leaching of U (c.f. section 7.2) imply interaction with oxygenated water, a central question is the origin of such water. In general, three types of water have been in contact with the BAS 1 surface: glacial meltwater during warm-based glacial periods and during deglaciations (the duration of these interactions is estimated at 10 to 40 ka) porewater in the Baltic sediments (≈ 6 ka) and meteoric water during the period of exposure (the last ≈ 4 ka).

Although it is difficult to determine the relative contribution of these water types to the oxidation/mobilisation of U and alteration of pyrite, glacial meltwater may have contributed significantly since it has been in contact with the BAS 1 surface for a longer period of time compared to Baltic pore water and meteoric water. Moreover, reducing condition probably developed in the Baltic sediments, and the interaction with meteoric water has been intermittent. The high content of oxygen and low content of dissolved solids (e.g. Cs) in meltwater would favour oxidation and mobilisation of U as well as desorption and mobilisation of Cs. It should, however, be pointed out that oxidation of pyrite is only seen in grains located within 0.5–1.0 mm of the surface whereas the oxidative leaching of U is traced to 20 mm depth. This indicates that oxidation of pyrite may be a slower process than oxidation/leaching of uranium, that mobilisation of U may take place under less oxidising conditions or that uranium is more easily accessible; for example, hosted in secondary mineral phases in microfractures and along grain boundaries. The latter is supported by results from leaching experiments in the field showing uranium mobilisation from a granitic bedrock surface /Strandh, 1999/.

In contrast to the situation at the outcropping surface at BAS 1, the results from the YA 1192 core show deposition of uranium ($^{234}U/^{238}U > 1$), unaltered pyrite in the fracture coating and pore water salinity similar to, or higher than, the present salinity in fracture groundwater at corresponding depth. This implies reducing conditions and, importantly, no evidence of intrusion of oxygenated glacial meltwater. Similar results ($^{234}U/^{238}U > 1$ and well-preserved pyrite) are also obtained in a study of the EW-1 zone at 60 metres depth at Äspö /Tullborg and Smellie, in manuscript/.

8 Concluding remarks

Two cores of the same rock type (Äspö diorite) have been studied and compared. The YA 1192 core was drilled from a water conducting fracture exposed in the Äspö tunnel at 170 m depth and the BAS 1 core from a glacially polished bedrock surface outcrop. The YA 1192 core shows the intercepted fracture to be characterised by a thin (< 1 mm) coating and an adjacent 2–3 cm hydrothermally altered zone and the BAS 1 core is characterised by a thin (< 0.5 cm) weathered surface rim and increase in microfractures in a 2 cm zone below the outcrop surface.

Retardation of U and Cs by matrix diffusion is indicated in the YA 1192 core. The diffusion is restricted to the hydrothermally altered zone, where increased porosity and the presence of saline water and sorbing secondary minerals occupying and lining the pores respectively, favour matrix diffusion retardation. In crystalline rocks such altered zones usually surround water-conducting fractures and their width (mostly in the order of 2–4 cm) probably sets a realistic limit for the matrix diffusion of the important radioactive waste radionuclides considering their half-lives. Parameter data of altered zones (depth, extension, porosity and distribution of microfractures and sorbing secondary phases) are thus important in modelling matrix diffusion retardation.

In BAS 1, alteration of pyrite has occurred in the weathered outcrop surface rim, and bulk leaching of U (as well as leaching of Cs) is indicated in a 2 cm zone below the outcrop surface. Both processes are confined to the last glacial/post-glacial period (approx. 100 ka) and demonstrate an oxidising environment and interaction with oxygenated water. According to the general opinion, glacial meltwater is characterised by a high content of oxygen and low content of dissolved solids thus being capable of oxidation/mobilisation of U, oxidation/alteration of pyrite and desorption/mobilisation of Cs. Glacial meltwater has certainly been in contact with the BAS 1 outcrop surface and most probably has been active in these processes. It is, however, difficult to distinguish between interactions of glacial meltwater and meteoric water, the latter having being active within the last 4 ka. Moreover, if glacial warm-based ice conditions (allowing for glacial meltwater interactions) has changed to cold-based ice conditions, the weathered zone may be removed by physical erosion/abrasion (caused by rock debris frozen in the bottom of the moving ice).

Based on the results from BAS 1, and site-specific data from Palmottu /Suksi and Raisilainen, 2000/ and Lac de Bonnet /Gascoyne and Cramer, 1987/, it is suggested that alteration of pyrite and bulk leaching of U are common results of interaction between oxygenated water and the uppermost bedrock surface or in near-surface fractures in areas influenced by the last glaciation. Depletion of U, $^{234}U/^{238}U \cong 1$, $^{230}Th/^{234}U > 1$ and alteration of pyrite (and formation of FeOOH) may thus be used as indicators of interaction with oxygenated surface waters (e.g. glacial meltwater during glaciation/deglaciations and meteoric water during interstadial/interglacial periods). Thus, it is concluded that the accumulation of U in the wall rock of the YA 1192 fracture, combined with the presence of fresh pyrite in the outermost coating, implies that intrusion of oxygenated surface water has not occurred in this fracture (170 m depth).

These results have an important implication in interpreting the palaeoevolution of the Äspö site as a whole. For example, components of groundwater with glacial meltwater signatures ($\delta^{18}O$ values varying from –15.8 to –13.6 per mil) found at depths from 134 to 450 m at Äspö /Laaksoharju et al., 1999/ may suggest that oxidising glacial waters have penetrated to these levels. However, results from this study and mineralogical results compiled in Tullborg /1997 and references therein) show that oxidising processes associated with glacial meltwater intrusion did not occur at these depths. This means that previous suggestions about a high O_2 content in glacial meltwaters may be over-estimated or, more probably, that the O_2 was consumed already in the near surface zone (0–50 m).

9 Acknowledgements

Leif Stenberg, Äspö Hard Rock Laboratory and Allan Stråhle Geosigma AB are acknowledged for their assistance in the selection of the sites and the drilling of the boreholes used in this study. Peter Wikberg, SKB and John Smellie, Conterra AB, have contributed constructive comments to the manuscript. Kristina Wiberg, Ritblocket made the drawings.

10 References

Alexander W R, Mackenzie A B, Scott R D, McKinley I G, 1990. Natural analogue studies in crystalline rock: The influence of water-bearing fractures on radionuclide immobilisation in a granitic rock repository. Nagra Technical Report 87-08, Switzerland.

Banwart S, Gustafsson E, Laaksoharju M, Nilsson A-C, Tullborg E-L, Wallin B, 1994. Large scale intrusion of shallow water into a vertical fracture zone in crystalline bedrock: Initial hydrochemical perturbation during the tunnel construction at the Äspö Hard Rock Laboratory, southeastern Sweden. Water Resources Research. 30, 1747–1763.

Berger A, Loutre M-F, 1997. Paleoclimate sensitivity to CO_2 and insolation. Ambio, 26, 32–37.

Björck S, 1995. A review of the history of the Baltic Sea, 13.0–8.0 ka BP. Quaternary International. 27, 19–40.

Byegård J, Johansson H, Skålberg M, Tullborg E-L, 1998. The interaction of sorbing and non-sorbing tracers with different Äspö rock types. SKB TR-98-18, Swedish Nuclear Fuel and Waste Management Co.

De la Roche H, Leterrier J, Grande Claude P, Marchal M, 1980. A classification of volcanic and plutonic rocks using R1-R2 diagrams and major element analyses – its relationships and current nomenclature. Chemical Geology, 29: 183–210.

Eliasson T, 1993. Mineralogy, geochemistry and petrophysics of red coloured granite adjacent to fractures. SKB TR 93-06, Swedish Nuclear Fuel and Waste Management Co.

Gaál G, Gorbatschev R, 1987. And outline of the Precambrian evolution of the Baltic Shield. Precambrian Research. 35, 15–52.

Gascoyne M, 1996. Highly saline pore fluids in the rock matrix of a granitic batholith on the Canadian Shield. Abstract., 30th Int. Geol. Congr., Beijing China (August 1996).

Gascoyne M, 1999. Long-term maintenance of reducing conditions in a spent fuel repository. A re-examination of critical factors. SKB R-99-41, Swedish Nuclear Fuel and Waste Management Co.

Gascoyne M, Schwarcz H P, 1986. Radionuclide migration over recent geologic time in a granitic pluton. Isotope Geoscience, 59, 75–85.

Gascoyne M, Cramer J J, 1987. History of actinide and minor element mobility in an Archean granitic batholith in Manitoba, Canada. Applied Geochemistry. 2, 37–54.

Glynn P D, Voss C I, Provost A M, 1999. Deep penetration of oxygenated meltwaters from warm based ice-sheets into the Fennoscandian Shield. Proceedings NEA/OECD Workshop on "Use of Hydrochemical Information in Testing Groundwater Flow Models", Borgholm, Sweden, Sept. 1–3, 1997.

Gorbatschev R, 1980. The Precambrium development of southern Sweden. GFF, 102, 129–136.

Govindajaru K, 1989. Geostandards Newsletter. 13, Special Issue, July 1989.

Guimerà L D, Jordana S, Bruno J, 1999. Effects of ice melting and redox front migration in fractured rocks of low permeability. SKB TR 99-19, Swedish Nuclear Fuel and Waste Management Co

Heath M J, Montoto M, 1996. Rock matrix diffusion as mechanism for radionuclide retardation: Natural radio-element migration in relation to the microfractography and petrophysics of fractures crystalline rock. EU-report EUR 17121 EN.

Imbrie J, Imbrie J Z, 1980. Modelling the climatic response to orbital variations. Science, 207, 943–953.

Johansson H, Siitari-Kauppi M, Skålberg M, Tullborg E-L, 1998. Diffusion pathways in crystalline rock – examples from Äspö diorite and fine-grained granite. Journal of Contaminant Hydrology 35, 41–53.

King-Clayton L M, Chapman N A, Kautsky F, Svensson N-O, Marsely G, Ledoux M, 1995. The central scenario for SITE-94: A climate change scenario. Swedish Nuclear Power Inspectorate SKI Report 95:42.

Kornfält K A, Persson P O, Wikman H, 1997. Granitoids from the Äspö area, SE Sweden – Geochemical and Geochronological data. Geologiska Föreningens i Stockholm Förhandlingar 114, 459–461.

Landström O, Tullborg E-L, 1994. Lithology, mineralogy and geochemistry of the Äspö bedrock and fracture fillings. Proceedings of the Äspö international geochemistry workshop, June 2–3, 1994. SKB ICR-94-13, Swedish Nuclear Fuel and Waste Management Co. ISSN 1104–3210.

Landström O, Tullborg E-L, 1995. Interactions of trace elements with fracture filling minerals from the Äspö Hard Rock Laboratory. SKB TR 95-13, Swedish Nuclear Fuel and Waste Management Co.

Laaksoharju M, Tullborg E-L, Wikberg P, Wallin B, Smellie J, 1999. Hydrogeochemical conditions and evolution at the Äspö HRL, Sweden. Applied Geochemistry, 14, 835–859.

Lidmar-Bergström K, 1995. Relief and saprolites through time in the Baltic Shield. Geomorphology, 12, 45–61.

Lång L-O, 2000. Heavy mineral weathering under acidic soil conditions. Applied Geochemistry, 15, 415–423.

Maddock R H, Hailwood E A, Rhodes E J, Muir Wood R, 1993. Direct fault dating trials at the Äspö hard rock laboratory. SKB TR 93-24, Swedish Nuclear Fuel and Waste Management Co.

Malmström M, Banwart S, Duro L, Wersin P, Bruno J, 1995. Biotite and chlorite weathering at 25° C. SKB TR 95-01, Swedish Nuclear Fuel and Waste Management Co, 128 p.

Miller W, Alexander R, Chapman N, McKinley I, Smellie J, 1994. Natural analogue studies in the geological disposal of radioactive waste. Studies in Environmental Science 57. Elsevier, Amsterdam. ISBN 0-444-81755-7.

Munier R, 1993. Segmentation, fragmentation and jostling of the Baltic shield with time. Thesis, Acta Universitatus Upsaliensis 37.

Neretnieks I, 1980. Diffusion in the rock matrix: an important factor in radionuclide migration? Journal of Geophysical Research, 85, 4379–4397.

Nesbitt H W, 1979. Mobility and fractionation of REE during weathering of granodiorite. Nature, 279, 206–210.

Nisca D H, 1987. Aerophysical interpretation. In SKB PR 25-87-04, Swedish Nuclear Fuel and Waste Management Co.

Nordström D K, Lindblom S, Donahoe R J, Barton C C, 1989. Fluid inclusions in the Stripa granite and their possible influence on the groundwater chemistry. Geochemica et Cosmochimica Acta, v. 53, p. 1741–1755.

Ota K, Amano K, Ando T, Sato H, Shibutani T, Tachi Y, 1997. In situ Matrix Diffusion in Fractured Crystalline rock, Kamaishi, in situ test site, North-East Japan. In: 6th International Conference on the Chemistry and Migration Behaviour of Actinides and Fission Products in Geosphere. Abst. Migration '97, Sendai, Japan, 26–31 Oct. 1997, 98–99.

Puigdomenech I, Ambrosi J-P, Banwart S A, Bateman K, Eisenlohr L, Gustafsson E, Hama K, Kotelnikova S, Lartige J-E, Michaud V, Milodowski A E, Pedersen K, Rivas Perez J, Trotignon L, Tullborg E-L, West J M, Yoshida H, 2001. O_2 depletion in granitic media: the REX project. SKB TR-01-05, Swedish Nuclear Fuel and Waste Management Co.

Siitari-Kauppi M, Marcos N, Klobes P, Goebbels J, Timonen J, Hellmuth K-H, 1999. Physical rock matrix characterization. The Palmottu Natural Analogue Project Report.

Smellie J A T (Editor), 2000. Matrix Fluid Experiment: Status Report (June 1998–June 2000). SKB Äspö Hard Rock Laboratory, International Collaboration Report IPR 00-35, Swedish Nuclear Fuel and Waste Management Co.

Smellie J A T, Stuckless J S, 1985. Element mobility studies of two drillcores from the Götemar granite, southeast Sweden. Chemical Geology, 51, 55–78.

Smellie J A T, MacKenzie A B, Scott R D, 1986. An analogue validation study of natural radionuclide migration in crystalline rocks using U-series disequilibrium studies. Chemical Geology, 55, 233–254.

Strandh H, 1999. Mineral dissolution from molecular to field scale. Ph D thesis, Department of Geology and Geochemistry No 304, ISSN 1101–1599.

Suksi J, Rasilainen K, 2000. Isotopic fractionation of U in rocks reflecting redox conditions around a groundwater flow route. Mat. Res. Soc. Symp. Proc. (in print).

Suksi J, Ruskeeniemi T, Rasilainen K, 1992. Matrix diffusion – evidences from natural analogue studies at Palmottu in SW Finland. Radiochimica Acta 58/59, 385–393.

Swantesson J O H, 1992. Recent microweathering phenomena in southern and central Sweden. Permafrost and Periglacial Processes, 3, 275–292.

Tirén S, Beckholmen M, 1987. Structural analysis of contoured maps Äspö and Ävrö, Simpevarp area. SKB PR 25-87-22, Swedish Nuclear Fuel and Waste Management Co.

Tullborg E-L, 1997. Recognition of low temperature processes in the Fennoscandian shield. Ph D thesis, Earth Science Centre A17, Göteborg University, ISSN 1400–3813.

Tullborg E-L, Larson S Å, Björklund L, Samuelsson L, Stigh J, 1995. Thermal evidence of Caledonide foreland, molasses sedimentation in Fennoscandia. SKB TR 95-18, Swedish Nuclear Fuel and Waste Management Co.

Tullborg E-L, Larson S Å, Stiberg J-P, 1996. Subsidence and uplift of the present land surface in the southern part of the Fennoscandian Shield. GFF, 112, 215–225.

Åberg G, Löfvendahl R, Levi B, 1984. The Götemar granite – isotopic and geochemical evidence for a complex history of an anorogenic granite. GFF, 106, 327–333.